nature plants

Article

https://doi.org/10.1038/s41477-024-01781-1

A sucrose ferulate cycle linchpin for ferulyolation of arabinoxylans in plant commelinids

Received: 12 October 2023

Accepted: 1 August 2024

Published online: 04 September 2024

Check for updates

A list of authors and their affiliations appears at the end of the paper

A transformation in plant cell wall evolution marked the emergence of grasses, grains and related species that now cover much of the globe. Their tough, less digestible cell walls arose from a new pattern of cross-linking between arabinoxylan polymers with distinctive ferulic acid residues. Despite extensive study, the biochemical mechanism of ferulic acid incorporation into cell walls remains unknown. Here we show that ferulic acid is transferred to arabinoxylans via an unexpected sucrose derivative, 3,6-*O*-diferuloyl sucrose (2-feruloyl-*O*-α-D-glucopyranosyl-(1′→2)-3,6-*O*-feruloyl-β-D-fructofuranoside), formed by a sucrose ferulate cycle. Sucrose gains ferulate units through sequential transfers from feruloyl-CoA, initially at the *O*-3 position of sucrose catalysed by a family of BAHD-type sucrose ferulic acid transferases (SFT1 to SFT4 in maize), then at the *O*-6 position by a feruloyl sucrose feruloyl transferase (FSFT), which creates 3,6-*O*-diferuloyl sucrose. An FSFT-deficient mutant of maize, *disorganized wall 1* (*dow1*), sharply decreases cell wall arabinoxylan ferulic acid content, causes accumulation of 3-*O*-feruloyl sucrose (α-D-glucopyranosyl-(1′→2)-3-*O*-feruloyl-β-D-fructofuranoside) and leads to the abortion of embryos with defective cell walls. In vivo, isotope-labelled ferulic acid residues are transferred from 3,6-*O*-diferuloyl sucrose onto cell wall arabinoxylans. This previously unrecognized sucrose ferulate cycle resolves a long-standing mystery surrounding the evolution of the distinctive cell wall characteristics of cereal grains, biofuel crops and related commelinid species; identifies an unexpected role for sucrose as a ferulate group carrier in cell wall biosynthesis; and reveals a new paradigm for modifying cell wall polymers through ferulic acid incorporation.

Cell walls are crucial to plant shape, strength and defence, as well as extensibility during growth and development[1–3]. The evolution of cell walls included a transformation in structure that marked the rise of grasses, grains and related species (Commelinids) now covering much of the Earth[4]. The grass cell wall is characterized by a novel pattern of interwoven arabinoxylan strands cross-linked with ferulate units that increase cellular toughness and resistance to digestion[5–7]. The primary (first-formed) cell walls of most land plants share foundational networks of cellulose microfibrils interlaced with hemicellulose chains and pectins, and the secondary walls are rigidified by lignin[8–12]. However, the evolution of the grass cell wall restructured this primary network by changing the hemicellulose composition and by cross-linking of ferulate moieties. In grass, hemicelluloses with 6-C xyloglucan backbones were largely replaced by 5-C arabinoxylans ((G)AX). The (G)AX backbones (β-1-4-linked-xylosyl units) carry side groups of α-1,2- and α-1,3-arabinofuranose that can be further modified at their

e-mail: bctan@sdu.edu.cn

O-5 position by *p*-coumarate (*p*CA) and ferulate esters that impart new properties[13]. Importantly, the ferulate units are oxidatively coupled to form covalent bonds within and between arabinoxylans and lignin[14,15]. 5–5-, 8–*O*–4-, 8–5- and 8–8-coupled ferulate dimers have been identified from grasses, as well as ferulate trimers and tetramers[16–18]. Cross-linking of ferulate units provides the cell walls of grass with enhanced rigidity and strength, pivotal to pathogen and herbivore resistance[19,20]. At the same time, ferulate cross-linking poses a challenge to economic uses of these species as forage crops, biofuel sources and feedstocks for designer biopolymers due to their resistance to digestion[21–23].

Intensive interest has thus been focused on the mechanism of ferulic acid (FA) addition to arabinoxylan (G)AX strands, though the process has resisted definition by even the most creative approaches. Thus far, evidence indicates that FA additions and oxidative coupling can occur in both the cytoplasm and the cell wall[24–26]. The FA donor was long thought to be feruloyl-CoA (Fer-CoA). Although the predicted transfer of the ferulate group from Fer-CoA to (G)AX substrates has been detected in extracts of rice cell cultures[26], the hypothesized arabinoxylan feruloyl transferase has eluded discovery. Phylogenetic analyses of grass genomes have identified members of the BAHD family of acyl-transferases as candidates, including Os01g09010 and its orthologue in *Setaria viridis*[27–31]. Downregulation of *Disorganized wall 1* (*Dow1*) homologous genes in *Oryza sativa* and *Setaria viridis* significantly decreased AX feruloylation[31,32]. Silencing of *BdBAHD01* in *Brachypodium* stems decreased feruloylation much less, possibly due to higher expression of functionally redundant genes[31]. Rice *xax1* (*xylosyl arabinosyl substitution of xylan 1*) mutant plants are deficient in FA and coumaric acid attached to arabinosyl residues in xylan substituted with xylosyl residues[7,33]. Overexpression of *BAHD10*/Os*AT10* results in a 60% reduction in matrix polysaccharide-bound FA and an approximately 300% increase in *p*CA in rice leaves[34]. Silencing Sv*BAHD05* presented a decrease of up to 42% of ester-linked *p*CA and 50% of *p*CA-arabinofuranosyl[35]. However, the enzyme activity has not been demonstrated[31]. The BAHD (PF02458) enzymes have a conserved HXXXDG active site and a carboxy-terminal DFGWG motif[28]. Nevertheless, the mechanism by which ferulate units are added to (G)AX remains unknown.

Here we define the long-sought mechanism of FA transfer essential to the cell wall strengthening that accompanied the evolution of grasses, grains and other commelinids. The newly identified sucrose ferulate cycle requires an unexpected facet of sucrose biochemistry that allows function as an FA carrier (3,6-*O*-diferuloyl sucrose). Our analysis of feruloyl sucrose feruloyl transferase (FSFT) encoded by the maize *Dow1* and related BAHD transferase proteins, combined with isotope feeding experiments, reveals a sucrose ferulate cycle in the following steps. First, 3-*O*-Fer sucrose is formed using Fer-CoA as the donor; second, 3,6-*O*-diFer sucrose is synthesized from 3-*O*-Fer sucrose again using Fer-CoA as the donor; and third, the two Fer groups of 3,6-*O*-diFer sucrose may be transferred directly onto (G)AX arabinoxylans or pass the ferulate groups to a donor, and the regeneration of sucrose completes this previously unrecognized metabolic cycle.

Results

The *dow1* mutation disrupts cell wall formation in maize seeds

The *dow1-1* mutant was isolated from the UniformMu mutagenesis population in which the *Mutator* (*Mu*) transposons were used as the mutagen in the W22 inbred background in maize. The seed-lethal *dow1-1* mutant, which severely impairs embryo and endosperm development (Fig. 1a and Extended Data Fig. 1a,b), segregates as a Mendelian recessive mutation (wild type:*dow1-1*, 747:248, $P < 0.05$). Mutant embryos fail to form distinct leaf primordia and root meristems by 15 days after pollination (DAP) (Fig. 1b). Transmission electron microscopy of the *dow1-1* embryos revealed a disorganized cell wall with reduced electron density (Fig. 1c). Cell wall component analysis by 2 M NaOH hydrolysis[36] showed that the cell wall ester-linked FA content was decreased by ~3.8-fold, whereas levels of *p*CA rose by ~80-fold in the mutant embryo (Fig. 1d). A similar but less marked pattern was detected in the endosperm (Fig. 1e). As alkaline hydrolysis breaks the ester bond between FA and the other compounds, we analysed the cell wall hydroxycinnamate (HCA) conjugates by anhydrous mild acidolysis[37], which breaks glycosidic bonds and releases HCA-arabinofuranoside from arabinoxylans. The FA-arabinofuranoside (FA-Ara) content was decreased by ~8.1-fold, while the *p*-coumaroyl arabinofuranoside (*p*CA-Ara) content rose by ~9.4-fold in the *dow1* mutant embryo compared with the wild type (Fig. 1f). In the endosperm, the FA-Ara content was reduced by 33.1-fold in the *dow1* mutant, but the level of *p*CA-Ara was unchanged, indicating that the *dow1* mutant is impaired in cell wall feruloylation of arabinoxylans (Fig. 1g). The methanol-soluble compounds were extracted using 90% methanol and analysed by high-performance liquid chromatography (HPLC). Compared with the wild type, the *dow1-1* mutant embryos accumulated several unknown compounds (Fig. 1h,i). Of these, Peak 1, with a retention time of ~9.79 min, was the most accumulated.

Dow1 encodes a BAHD family acyltransferase

We cloned *Dow1* by transposon tagging[38]. The *dow1-1* allele carries a *Mu8* transposon insertion in the first exon of GRMZM2G314898 (Extended Data Figs. 1f and 2a), whereas the phenotypically similar *dow1-2* has a *Mu1* transposon insertion in the second exon (Extended Data Fig. 2a). Allelism was confirmed by genetic complementation tests establishing GRMZM2G314898 as the causal gene (Extended Data Fig. 1c,d). Subcellular localization of DOW1–GFP in maize protoplasts, *Arabidopsis* protoplasts and tobacco leaf epidermal cells showed that DOW1 is predominantly localized in the cytosol (Extended Data Fig. 2b). However, a partial association with the endoplasmic reticulum was indicated by western blot analysis of subcellular fractions using antibodies against DOW1 and an endoplasmic reticulum marker, the binding immunoglobulin protein (Extended Data Fig. 2c–e). *Dow1* transcripts are ubiquitously expressed in major organs of maize, with relatively high levels in silks, roots, bracts and flowers (Extended Data Fig. 2f).

DOW1 catalyses the synthesis of 3,6-*O*-diFer sucrose

The cell wall defects and reduced arabinoxylan-conjugated FA content in the *dow1* mutant suggest a role of DOW1 in transferring ferulate units to cell wall arabinoxylans. DOW1 belongs to the Pfam family PF02458 of the BAHD acyltransferase superfamily[27,28]. Ten BAHD acyltransferases in rice have been identified bioinformatically as candidates for arabinoxylan feruloylation, referred to as the Mitchell-clade proteins[27,28]. Phylogenetic analysis of the Mitchell-clade proteins in related species shows that DOW1 is closely related to Os01g09010 (*Os*BHAD1) in rice (Supplementary Fig. 1a). Other members include Fer-CoA:arabinofuranose transferase, *p*-coumaroyl-CoA:arabinofuranose transferase, Fer-CoA:monolignol transferase and *p*-coumaroyl-CoA:monolignol transferase[29,31,32,34,35,39–41] (Supplementary Fig. 1a). All the maize Mitchell-clade members contain the conserved HXXXDG and DYGWG motifs (Supplementary Fig. 1b).

To discover the biochemical function of DOW1, we purified recombinant MBP–DOW1 from *Escherichia coli* (Extended Data Fig. 1h). We tested the MBP–DOW1 activity using Fer-CoA as the ferulate group donor and 3^2-α-L-arabinofuranosyl-xylobiose (A3X) and 2^3-α-L-arabinofuranosyl-xylotriose (A2XX) as the feruloyl acceptors. However, no activity was detected in either reaction, suggesting that A3X and A2XX may not be the DOW1 substrates. We reasoned that the DOW1 substrate might be accumulated in the *dow1* mutant, considering the unknown compounds were indeed accumulated in *dow1* (Fig. 1h,i). We thus tested the MBP–DOW1 activity using the 90% methanol extracts from the *dow1-1* embryos as the substrate and Fer-CoA as the donor. Peak 1, the most accumulated compound in the *dow1-1* embryo extract, was unchanged regardless of whether it was incubated with or without Fer-CoA (Figs. 1h,i and 2a, trace 1). However, when the

https://doi.org/10.1038/s41477-024-01781-1

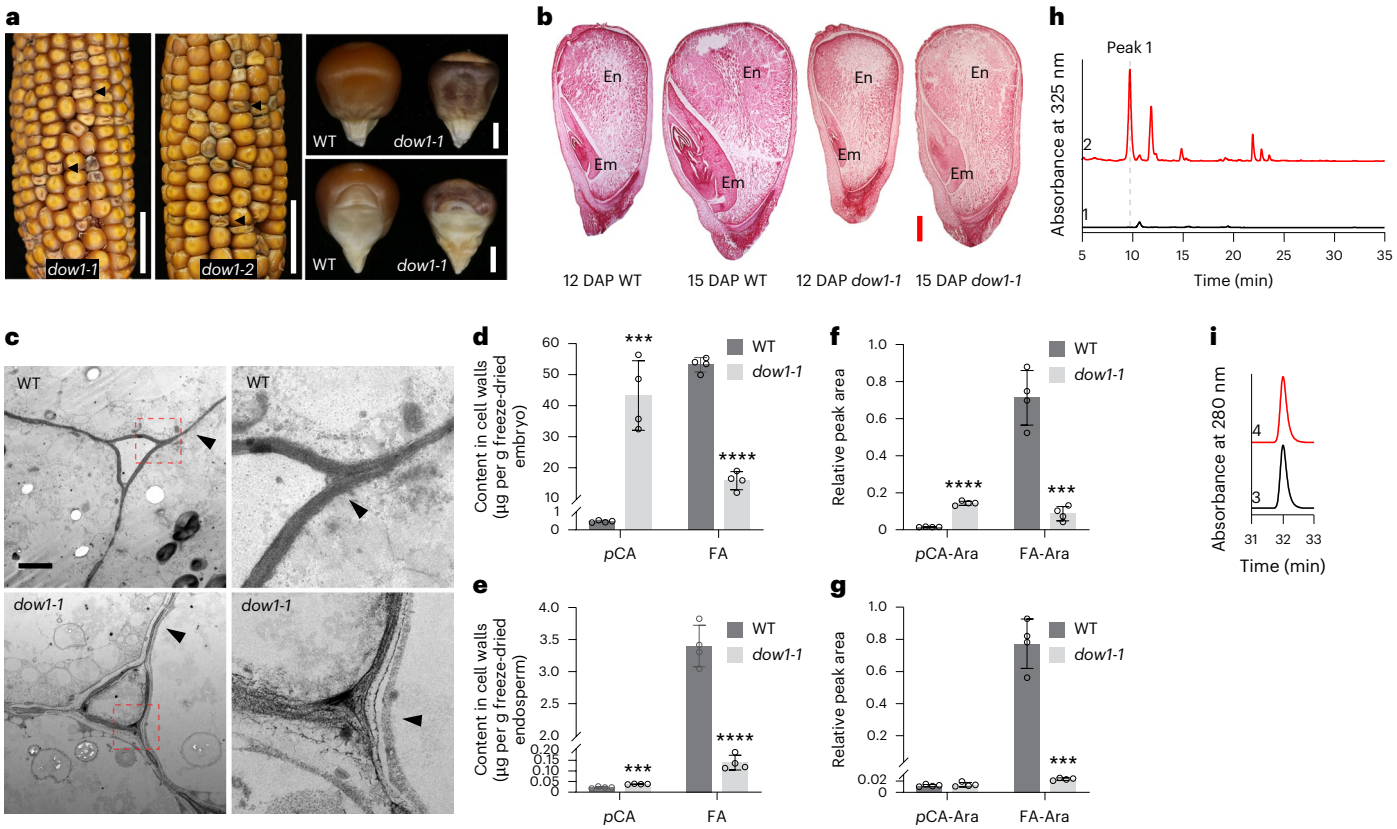

Fig. 1 | The maize *dow1* mutant has defective cell walls. a, Ears of self-pollinated, heterozygous *dow1-1* and *dow1-2* mutants (left), with germinal (bottom) and abgerminal (top) faces of *dow1-1* mutant kernels (right). Scale bars, 2 cm (ears) and 0.2 cm (kernels). The arrowheads point out the mutant kernels. **b**, Sections of developing wild-type (WT) and *dow1-1* kernels at 12 and 15 DAP. Scale bar, 1 mm. Em, embryo; En, endosperm. **c**, Transmission electron micrographs of wild-type and *dow1-1* embryos at 15 DAP reveal disorganized cell walls. Scale bar, 2 μm. The boxed areas are magnified in the right panels. The arrowheads point out the cell walls of the wild-type and the *dow1-1* mutant. The experiments were repeated independently with similar results at least three times. **d**,**e**, Ester-linked *p*CA and FA contents in cell walls of wild-type and *dow1-1* embryos (**d**) and endosperm (**e**). The error bars indicate the mean ± s.d. ($n = 4$ replicates of assays with independent plants). Two-tailed *P* values: $^{***}P = 0.0046$ (*p*CA content of embryo), $^{****}P < 0.000002$ (FA content of embryo), $^{***}P = 0.0016$ (*p*CA content of endosperm) and $^{****}P = 0.0039$ (FA content of endosperm) by Welch's unpaired *t*-test. **f**,**g**, HCA conjugate contents in cell walls of wild-type and *dow1-1* embryos (**f**) and endosperm (**g**). The relative peak areas of major peaks of *p*CA-Ara and FA-Ara are shown. The error bars indicate the mean ± s.d. ($n = 4$ replicates of assays with independent plants). Two-tailed *P* values: $^{****}P = 0.0001$ (*p*CA-Ara content of embryo), $^{***}P = 0.0023$ (FA-Ara content of embryo), $P = 0.4993$ (*p*CA-Ara content of endosperm) and $^{***}P = 0.0023$ (FA-Ara content of endosperm) by Welch's unpaired *t*-test. **h**, HPLC analysis of 90% methyl alcohol extracts from 15 DAP wild-type (trace 1) and *dow1-1* mutant (trace 2) embryos. **i**, A spiked-in internal standard of 0.08 mM cinnamic acid in the wild-type (trace 3) and *dow1-1* (trace 4) for the 90% methyl alcohol extraction.

extract was incubated with Fer-CoA and MBP–DOW1, a concurrent decrease in Peak 1 and an increase in Peak 2 occurred, indicating that MBP–DOW1 converted Peak 1 to Peak 2 in vitro (Fig. 2a, trace 2).

As Peak 2 holds the key to unlocking the function of DOW1, we sought to resolve the structure of Peak 2. Large-scale preparation of Peak 2 was achieved using the reaction described in Fig. 2a (trace 2). Peak 2 (5 mg) was purified to nearly 100% purity (Supplementary Fig. 5f, trace 2) and then analysed using HPLC–high-resolution mass spectrometry/mass spectrometry (HPLC–HR-MS/MS) and nuclear magnetic resonance (NMR). The chemical structure of Peak 2 was identified as 2-feruloyl-*O*-α-D-glucopyranosyl-(1′→2)-3,6-*O*-feruloyl-β-D-fructofuranoside (3,6-*O*-diFer sucrose) with observed 693.2003 $[M\text{-}H]^-$ versus calculated 693.2025 for $C_{32}H_{37}O_{17}$ (Fig. 2f and Supplementary Figs. 2 and 5; refer to Methods for the details). The detailed one-dimensional and two-dimensional NMR spectral analysis of 3,6-*O*-diFer sucrose (Peak 2) is provided in Supplementary Fig. 6 and Supplementary Table 1. In addition, the HR-MS and NMR data are fully consistent with properties of 3,6-*O*-diFer sucrose isolated from *Heloniopsis orientalis*, *Paris polyphylla* var. *yunnanensis* and rice biochemically[42–45]. Similarly, Peak 1 was found to be α-D-glucopyranosyl-(1′→2)-3-*O*-feruloyl-β-D-fructofuranoside, or 3-*O*-feruloyl sucrose (3-*O*-Fer sucrose), which is also named sibiricose A5 (Fig. 2f and Supplementary Fig. 3). Peak 1 has a retention time identical to that of sibiricose A5 in the HPLC analysis (Figs. 1h and 2a,b). We further confirmed that Peak 1 is 3-*O*-Fer sucrose by using sibiricose A5 and Fer-CoA as the substrates; MBP–DOW1 converted sibiricose A5 to 3,6-*O*-diFer sucrose (Peak 2) (Fig. 2b). DOW1 is thus an FSFT that catalyses transfer of the ferulate residue from Fer-CoA to the *O*-6 position of 3-*O*-Fer sucrose to produce 3,6-*O*-diFer sucrose. Michaelis–Menten plots show that DOW1 displays typical enzymatic kinetics, yielding $K_m = 0.098$ mM for 3-*O*-Fer sucrose and $K_m = 0.118$ mM for Fer-CoA (Fig. 2d,e). When Peak 2 was in turn incubated with a cell membrane fraction (CMF) from the wild-type kernels, Peak 2 was converted to Peak 3 and FA (Fig. 2c). Structural analysis reveals that Peak 3 is 6-*O*-Fer sucrose (α-D-glucopyranosyl-(1′→2)-6-*O*-feruloyl-β-D-fructofuranoside) (Fig. 2f and Supplementary Fig. 4). Hence, DOW1 catalyses the synthesis of 3,6-*O*-Fer sucrose from 3-*O*-Fer sucrose, and 3,6-*O*-Fer sucrose can be converted to 6-*O*-Fer sucrose by an unknown enzyme (Fig. 2f).

SFT1, SFT2, SFT3 and SFT4 catalyse the synthesis of 3-*O*-Fer sucrose

As 3-*O*-Fer sucrose (Peak 1) is the substrate of DOW1, which is accumulated in the *dow1* mutant, we next attempted to identify the enzyme

https://doi.org/10.1038/s41477-024-01781-1

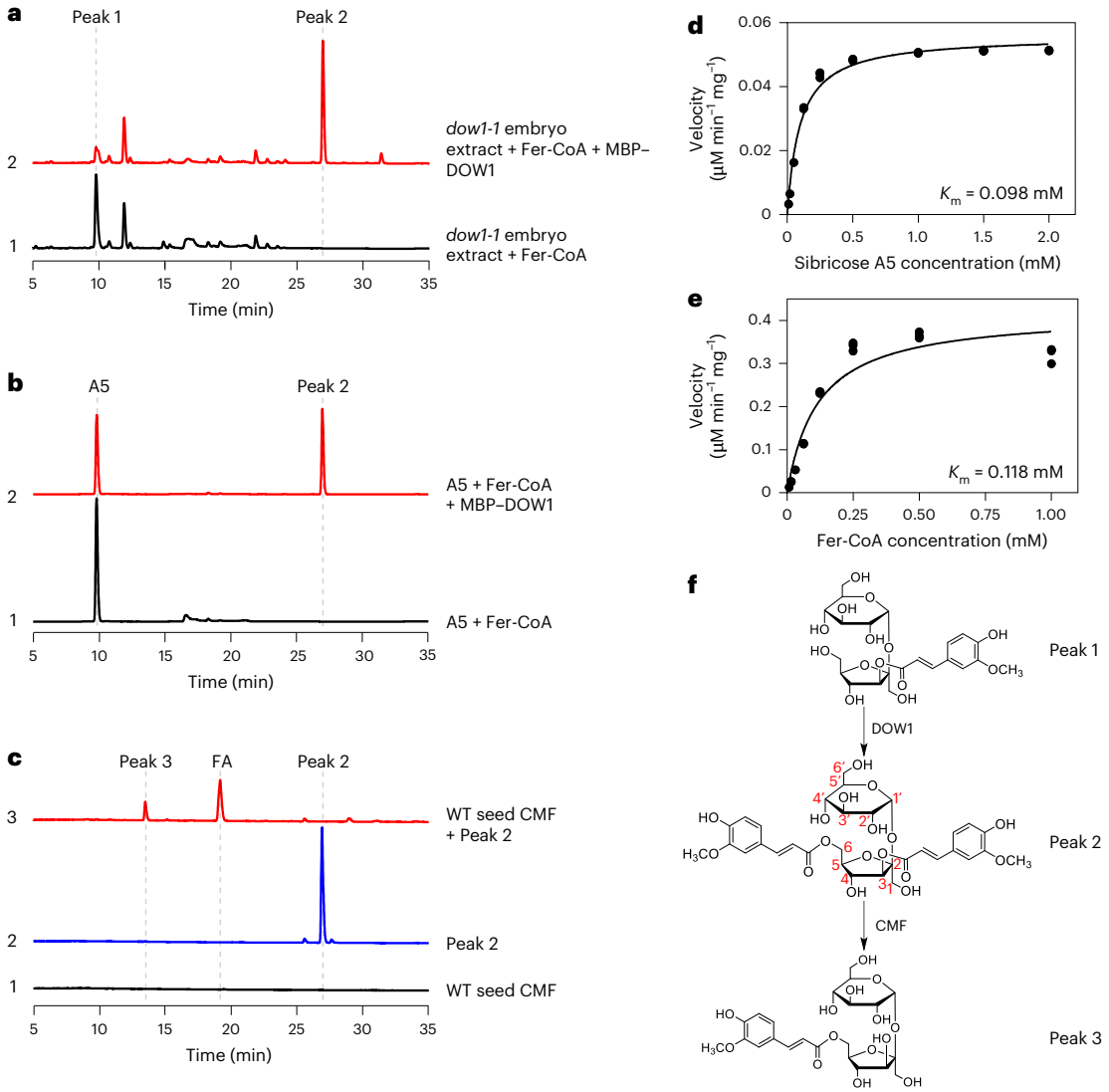

Fig. 2 | Conversion of Peak 1 to Peak 2 by transfer of FA from Fer-CoA catalysed by recombinant MBP–DOW1, and in vitro conversion of Peak 2 to Peak 3 mediated by a cell membrane extract from wild-type kernels. a, FSFT activity of DOW1 transfers Fer from Fer-CoA to Peak 1, forming Peak 2 in vitro. The HPLC trace 1 analysis of 250 μM Fer-CoA and *dow1* embryo extract is compared to trace 2 analysis of the reaction products from 250 μM Fer-CoA, *dow1* embryo extract and 10 μg MBP–DOW1. The enzyme was assayed at 30 °C for 24 h. **b**, DOW1 FSFT activity catalyses the transfer of the ferulate group from Fer-CoA to sibiricose A5 (A5), forming Peak 2 in vitro. The HPLC trace 1 analysis of 500 μM Fer-CoA, 500 μM A5 and 10 μg MBP and the trace 2 analysis of the reaction products from 500 μM Fer-CoA, 500 μM A5 and 10 μg MBP–DOW1 are shown. The enzyme was assayed at 30 °C for 5 h. **c**, The CMF from the wild type contains an unknown protein that de-esterifies Peak 2 to form Peak 3 and FA in vitro. The HPLC trace 1 analysis of 200 μg wild-type kernel CMF, HPLC trace 2 analysis of 9 μM Peak 2 and HPLC trace 3 analysis of the reaction products from 200 μg wild-type seed CMF with 9 μM Peak 2 are shown. The enzyme was assayed at 30 °C for 24 h. **d**,**e**, Determination of the K_m value of ZmDOW1 using a Michaelis–Menten plot. The K_m value represents the mean of three replicates of assays with independent proteins. **f**, Chemical structures of Peak 1, Peak 2 and Peak 3.

catalysing the synthesis of Peak 1. We speculated that the reaction probably involves the transfer of the ferulate group from Fer-CoA to sucrose, and the Mitchell-clade proteins in maize would be the best candidates[27]. We named this enzyme sucrose:Fer-CoA feruloyl transferase (SFT). To this end, each of the Mitchell-clade genes in maize was cloned and expressed in *E. coli* as an MBP fusion protein. The recombinant proteins were purified (Extended Data Fig. 1h) and assayed with 1 mM sucrose and 250 μM Fer-CoA. As shown in Fig. 3a, SFT1 (GRMZM2G375159), SFT2 (GRMZM2G108714), SFT 3 (GRMZM2G060210) and SFT 4 (GRMZM2G159641) catalysed the synthesis of 3-*O*-Fer sucrose as indicated by the standard sibiricose A5. Michaelis–Menten plots confirmed the sucrose feruloyl transferase activities of SFT1, SFT2, SFT3 and SFT4 in typical enzymatic kinetics, with SFT1 having the lowest K_m value (Fig. 3b–e).

Ferulate units of 3,6-*O*-diFer sucrose are incorporated into arabinoxylans

To test whether the sucrose derivatives carrying one ferulate unit (6-*O*-Fer sucrose, Peak 3) or two (3,6-*O*-diFer sucrose, Peak 2) can donate Fer to cell wall arabinoxylans, we synthesized each compound with $^2H_3$-labelled ferulate groups, fed them to maize seedlings and analysed the [$^2H_3$]Fer incorporation into cell walls. To distinguish between the two ferulate groups in 3,6-*O*-diFer sucrose, we separately labelled the ferulate residues at the *O*-3 and *O*-6 positions, respectively, yielding 3-[$^2H_3$]Peak 2 (3-[$^2H_3$]P2) and 6-[$^2H_3$]Peak 2 (6-[$^2H_3$]P2). Isotope-labelled 6-[$^2H_3$]Peak 3 (6-[$^2H_3$]P3) was synthesized as described (Extended Data Fig. 3a–c), and its high purity was verified (Extended Data Fig. 3d–f). Equimolar 3-[$^2H_3$]P2, 6-[$^2H_3$]P2 and [$^2H_3$]FA and 2 × molar [$^2H_3$]FA were fed to maize seedlings grown in Murashige and Skoog medium. Because

https://doi.org/10.1038/s41477-024-01781-1

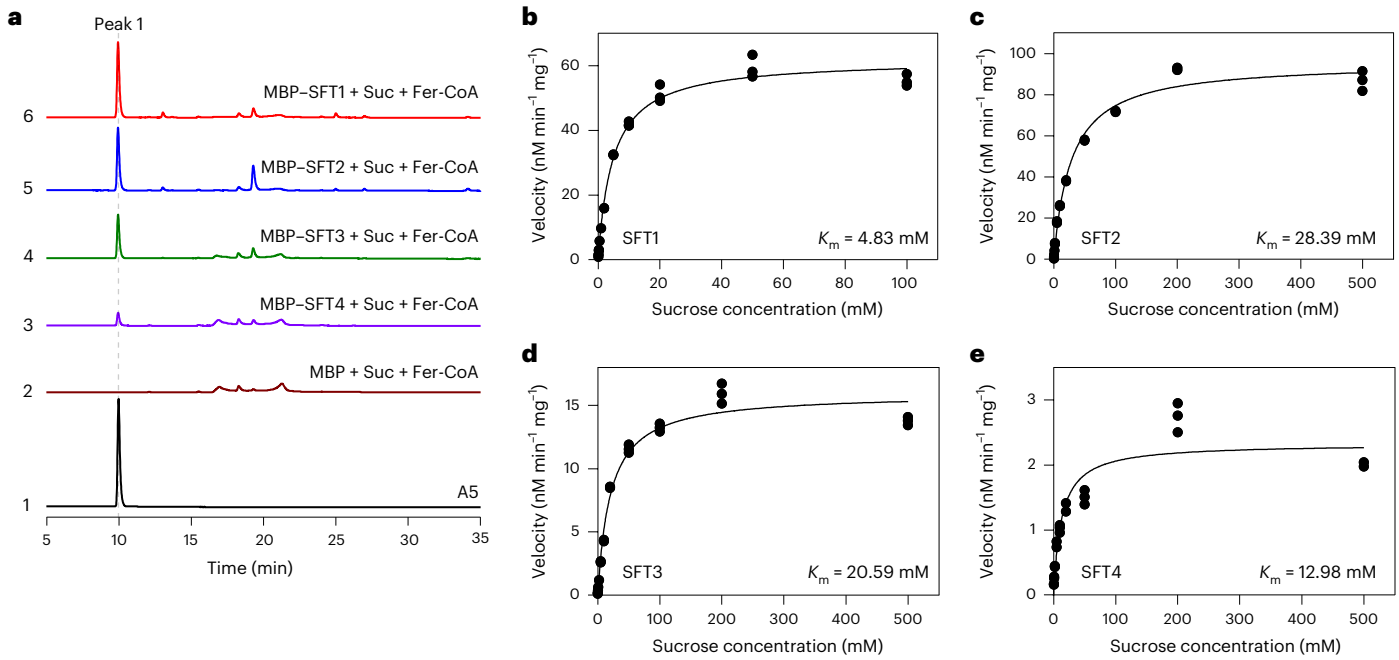

Fig. 3 | Recombinant BAHD transferases MBP–SFT1, MBP–SFT2, MBP–SFT3 and MBP–SFT4 catalyse the synthesis of 3-*O*-Fer sucrose (Peak 1) from Fer-CoA and sucrose. a, Products were quantified by HPLC after reaction of 1 mM sucrose (Suc), 250 µM Fer-CoA and 10 µg MBP with 10 µg recombinant MBP–SFT proteins in a 100 µl reaction mixture. The enzymes were assayed at 30 °C for 5 h. Recombinant proteins were purified from *E. coli* as MBP–SFT fusions. **b**–**e**, Determination of the K_m value of *Zm*SFT1 (**b**), *Zm*SFT2 (**c**), *Zm*SFT3 (**d**) and *Zm*SFT4 (**e**) using Michaelis–Menten plots. The K_m value represents the mean of three replicates of assays with independent proteins.

only a limited amount of 6-[$^2H_3$]P3 was synthesized, it was fed at a ½ molar scale. Methanol solvent was used as a control. After feeding, cell wall esterified FAs were extracted and analysed by HPLC–HR-MS.

FAs identified from the seedlings fed the labelled compounds are in several forms, including free FA monomer (FA) and dimers (diFA) with varying degrees of decarboxylation[46] (Extended Data Figs. 4, 5a,d, 6a,d, 7a,c, 8a,c and 9a,c). In plants fed either 3-[$^2H_3$]P2 or 6-[$^2H_3$]P2, $^2H_3$-labelled FA ([$^2H_3$]FA), single FA-labelled non-decarboxylated diFA ($^2H_3$-non-decarboxylated diFA), double FA-labelled non-decarboxylated diFA ($^2H_6$-non-decarboxylated diFA), single FA-labelled decarboxylated diFA ($^2H_3$-decarboxylated diFA) and double FA-labelled decarboxylated diFA ($^2H_6$-decarboxylated diFA) were observed in cell walls (Extended Data Figs. 4b,c, 5b–d and 6b–d). These labelled compounds were also recovered in the cell walls of seedlings fed 1 × molar [$^2H_3$]FA and 2 × molar [$^2H_3$]FA (Extended Data Figs. 4b,c, 5b–d and 6b–d). These results demonstrate that the ferulate residues at both the *O*-3 and *O*-6 positions of 3,6-*O*-diFer sucrose can be incorporated into the cell wall. Similarly, [$^2H_3$]FA, $^2H_3$-non-decarboxylated diFA and $^2H_3$-decarboxylated diFA were recovered in the cell walls of plants treated with ½ × molar 6-[$^2H_3$]P3 (Extended Data Figs. 7b,c, 8b,c and 9b,c). However, [$^2H_6$] diFA forms were not detected, possibly due to the low concentration of ½ × 6-[$^2H_3$]P3 applied to plants, as [$^2H_6$]diFA was also not detected in the plants fed ½ × [$^2H_3$]FA (Supplementary Fig. 8).

To test whether the ferulate group was incorporated into cell wall arabinoxylans, we analysed the cell wall HCA conjugates by mild acid-olysis of cell walls with 50 mM trifluoroacetic acid (TFA)[31], which breaks the glycosidic bonds and allows the detection of HCA conjugated to arabinose by HPLC–HR-MS. [$^2H_3$]FA-Ara and Ara-[$^2H_3$]FA-FA-Ara were detected in the cell walls of plants fed with 3-[$^2H_3$]P2, 6-[$^2H_3$]P2 and [$^2H_3$]FA (Fig. 4a,b) as indicated by the increased molecular weight of 328.1083 for [$^2H_3$-FA-Ara-H]$^-$ and 652.1954 for [Ara-$^2H_3$-FA-FA-Ara-H]$^-$. However, [$^2H_3$]FA-Ara and Ara-[$^2H_3$]FA-FA-Ara were not detected in plant cell walls treated with 6-[$^2H_3$]P3 (Extended Data Fig. 10). These results indicate that both ferulate groups of 3,6-*O*-diFer sucrose are incorporated into arabinoxylans, and the ferulate group of 6-*O*-Fer sucrose is not. Possibly, the ferulate group is incorporated into other components of the cell wall, as alkaline hydrolysis of cell wall HCA conjugates detected [$^2H_3$]FA (Extended Data Figs. 4–9 and Supplementary Fig. 7).

Discussion

Despite the pivotal importance of cell wall polymer cross-linking for plant growth, plant development, and herbivore and pathogen resistance of cereal grains as well as biofuel crops, the biochemical basis for synthesis of the grass cell wall has stymied researchers for decades. A key feature of this evolutionary transformation is the cross-linking of interwoven arabinoxylans mediated by regularly spaced ferulate units[4,27,47]. This innovation affects cells of commelinid plants, including grasses, grains, sedges, bromeliads and related species. Yet the biochemical mechanism of ferulate unit incorporation remains a mystery.

The key to solving the mystery is a new sucrose ferulate cycle revealed by molecular and biochemical analyses of maize *dow1* and related PF02458 family genes (Fig. 5). The essential role of a feruloylated sucrose intermediate, 3,6-*O*-diFer sucrose, establishes a new and unexpected role for sucrose as a ferulate group carrier in cell wall biosynthesis. Our results define the molecular functions of DOW1 (FSFT), SFT1, SFT2, SFT3 and SFT4 in the synthesis of diferulated sucrose and arabinoxylan feruloylation in maize. SFT1 through SFT4 are sucrose feruloyl transferases that catalyse the addition of one ferulate group from Fer-CoA to sucrose, generating 3-*O*-Fer sucrose (Fig. 3). DOW1, in turn, is an FSFT that catalyses the addition of a second ferulate group from Fer-CoA to 3-*O*-Fer sucrose, forming 3,6-*O*-diFer sucrose (Fig. 2a,b,d–f). The different specificities of SFT and FSFT enzymes explain the accumulation of 3-*O*-Fer sucrose in extracts of the *dow1* mutant (Fig. 1h,i). Furthermore, we demonstrated by isotope feeding experiments that the two ferulate groups of 3,6-*O*-diFer sucrose are incorporated into arabinoxylans in cell walls (Fig. 4, Extended Data Figs. 4–6 and Supplementary Fig. 7), explaining the severe impact of

https://doi.org/10.1038/s41477-024-01781-1

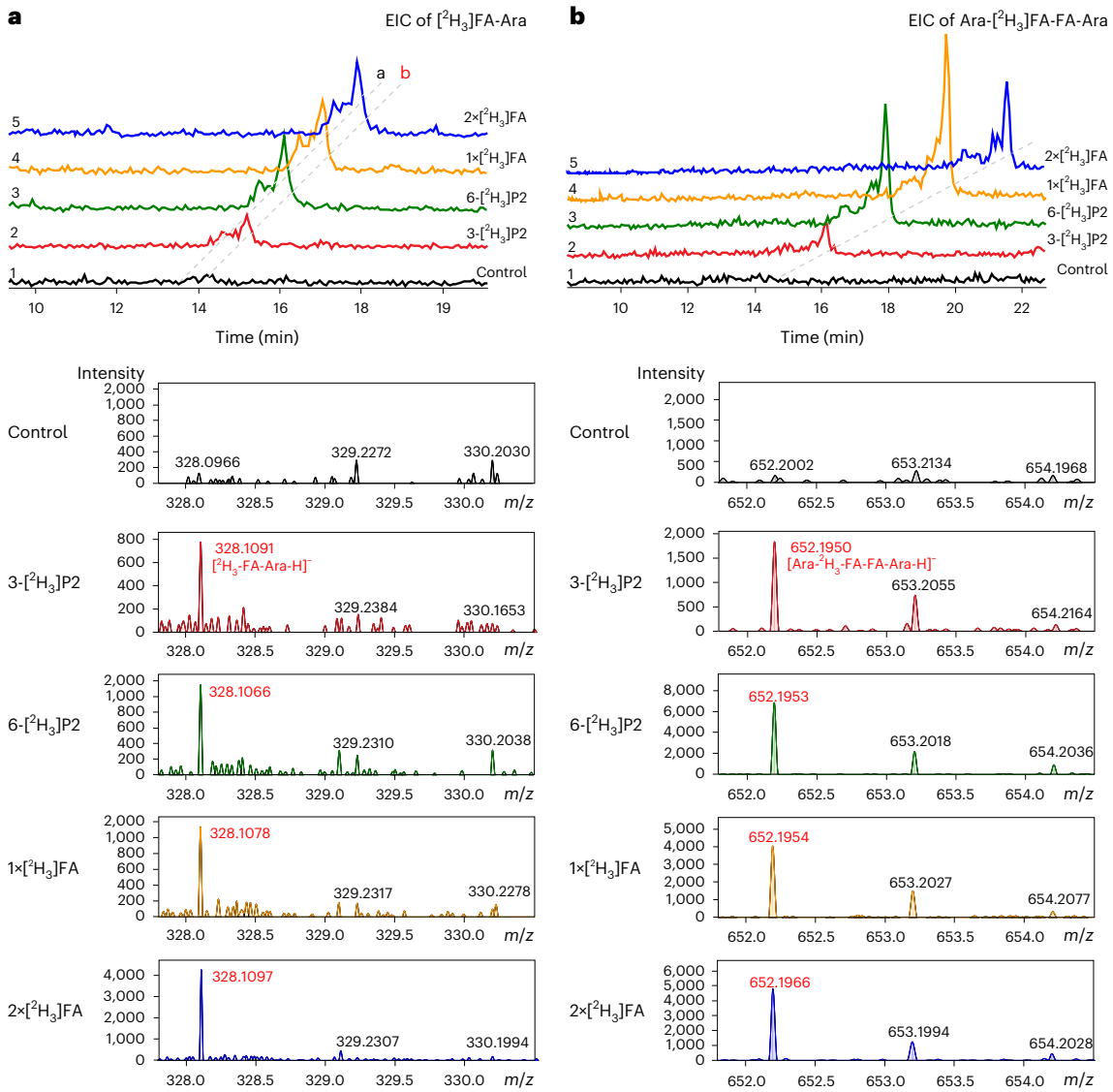

Fig. 4 | Incorporation of FA from sucrose 3,6-O-diFer sucrose (Peak 2) and intermediates into cell wall arabinoxylans. a,**b**, HPLC–HR-MS analysis quantified [$^2H_3$]FA-Ara and Ara-[$^2H_3$]FA-FA-Ara of cell wall arabinoxylans of control plants and seedlings fed isotope-labelled substrates by the 50 mM TFA mild acidolysis method. Panel **a** shows an extracted-ion chromatogram (EIC) and mass spectra of [$^2H_3$]FA-Ara (328.1106, $C_{15}H_{15}D_3O_8$, [M-H]$^-$) from traces unlabelled controls (trace 1) and seedlings fed with 13.9 μM 3-[$^2H_3$]P2 (2), 13.9 μM 6-[$^2H_3$]P2 (3), 13.9 μM [$^2H_3$]FA (4) or 27.8 μM [$^2H_3$]FA (5). **b**, An EIC and mass spectra of Ara-[$^2H_3$]FA-FA-Ara (652.1905, $C_{30}H_{31}D_3O_{16}$, [M-H]$^-$) from traces unlabelled controls (trace 1) and seedlings fed with 13.9 μM 3-[$^2H_3$]P2 (2), 13.9 μM 6-[$^2H_3$]P2 (3), 13.9 μM [$^2H_3$]FA (4) or 27.8 μM [$^2H_3$]FA (5). The ion chromatogram marked red shows the observed mass spectra of [$^2H_3$]FA-Ara from the treated seedlings.

loss of function of DOW1 on cell wall structure and reduced ferulate modification of arabinoxylans in the *dow1* mutant (Fig. 1c–g).

3,6-*O*-diFer sucrose either directly donates ferulate groups to arabinoxylans or passes the ferulate groups to a direct donor. In either case, we suggest that the ferulate group transfer follows a 3-*O*-Fer and 6-*O*-Fer order, as transfer of the 6-*O*-Fer would produce 3-*O*-Fer sucrose, which is the accumulated Peak 1 in the *dow1* mutant. 3,6-*O*-diFer sucrose can be converted to 6-*O*-Fer sucrose by an unknown enzyme in the CMF (Fig. 2c). [$^2H_3$]FA and [$^2H_3$]diFA were detected in the cell walls of plants fed 6-[$^2H_3$]P3, but [$^2H_3$]FA-Ara and Ara-[$^2H_3$]FA-FA-Ara were not detected (Extended Data Fig. 10), indicating that the ferulate group from 6-*O*-Fer sucrose was incorporated not into arabinoxylans but into other components of the wall.

On the basis of these results, we propose a sucrose ferulate cycle that synthesizes the diFer sucrose for Fer incorporation into arabinoxylans of cell walls (Fig. 5). In this cycle, the first FA group is transferred from Fer-CoA to the 3-*O* position of sucrose to form 3-*O*-Fer sucrose (Peak 1), a reaction catalysed by SFT1, SFT2, SFT3 and SFT4. A second ferulate group is transferred to the 6-*O* position of 3-*O*-Fer sucrose by DOW1 (FSFT) to generate 3,6-*O*-diFer sucrose (Peak 2). 3,6-*O*-diFer sucrose donates the ferulate groups to arabinoxylans or to a direct donor, regenerating sucrose and completing the cycle (Fig. 5). Identifying the feruloyl transferase that catalyses the ferulate group transfer from 3,6-*O*-diFer sucrose to an acceptor would clarify the donor question. In a separate route, 3,6-*O*-diFer sucrose can be converted to 6-*O*-Fer sucrose by an unknown enzyme in the CMF (Fig. 2c), which may donate its ferulate group to cell walls.

Fer-CoA has long been hypothesized to directly donate ferulate units to arabinoxylans of cell walls[26]. Hence, candidate BAHD (PF02458) family acyl transferases have been studied extensively in grasses[27]. The transfer of ferulate residues from Fer-CoA to arabinoxylan-trisaccharide (A3X) has indeed been detected, but only in the presence of cell wall or cytosolic fractions from cultured rice cells[26]. Our results indicate that Fer-CoA transferase activity measured in rice cell cultures can be

https://doi.org/10.1038/s41477-024-01781-1

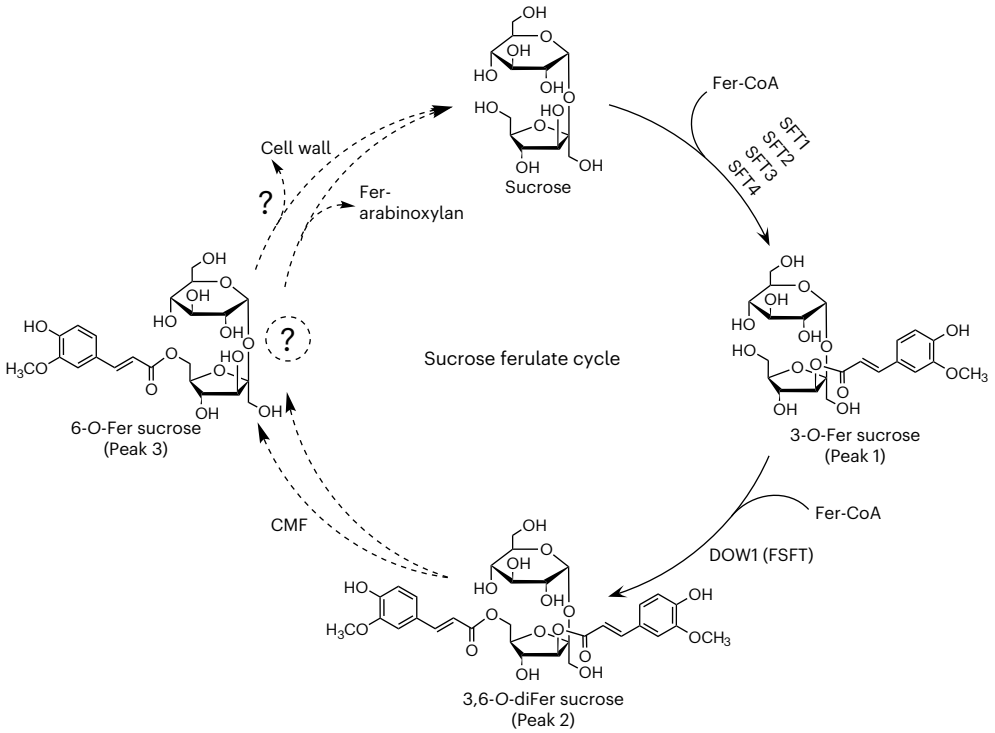

Fig. 5 | A proposed sucrose ferulate cycle required for ferulate incorporation into arabinoxylans of grass-type plant cell walls. Question marks represent unknown enzymes or compounds. Solid lines denote confirmed results, and dashed lines represent unconfirmed results.

explained if cell extracts include sucrose and enzymes of the sucrose ferulate cycle (Fig. 5).

Our data show that the donation of ferulate residues to cell wall arabinoxylans can be mediated by di-Fer sucrose intermediates appearing in Peak 2 (3,6-*O*-diFer sucrose) (Fig. 4, Extended Data Figs. 4–6 and Supplementary Fig. 7). We also investigated the possibility that the ferulate unit from 3,6-*O*-diFer sucrose or 6-*O*-Fer sucrose could be released as free FA by an esterase and then incorporated into the cycle in this form. However, our isotope-labelling data do not favour this scenario because 3-[$^2H_3$]P2 and 6-[$^2H_3$]P2 led to similar amounts of ferulate incorporation into cell walls (especially the FA dimer forms) (Extended Data Figs. 4–6). In addition, [$^2H_3$]FA was not detected in the 80% ethanol extract from plants treated with 6-[$^2H_3$]P2 (Supplementary Fig. 7c), and the ferulate group of 6-[$^2H_3$]P3 was not found incorporated into arabinoxylans (Extended Data Fig. 10). Our results thus support the hypothesis that 3,6-*O*-diFer sucrose serves as a donor of ferulate groups to arabinoxylans in cell walls. By contrast, 3-*O*-Fer sucrose is not an effective donor on its own, as it accumulates in the *dow1-1* mutant (Fig. 1h,i), which is deficient in arabinoxylan feruloylation in the cell wall (Fig. 1f,g).

Thus far, 3-*O*-Fer sucrose is the only known substrate for DOW1 (FSFT). We tested whether other carbohydrates and polysaccharides, including A3X, A2XX, uridine diphosphate glucose, glucose, uridine diphosphate arabinose and arabinose could serve as recipients of the FA group from Fer-CoA in the DOW1 reaction. None of these compounds were substrates. The identification of sucrose as an unexpected carrier for ferulate group transfer to arabinoxylans in the cell wall reveals a new mechanism of sucrose input into plant growth and cell wall extensibility. The distinctive mechanism and resulting linkages are pivotal in three ways. First, they define an evolutionary transformation of the plant cell wall that increased the strength, rigidity and herbivore resistance of the widely successful commelinid species (grasses, grains, sedges, bromeliads and beyond). Second, the newfound role of sucrose and associated enzyme activities open unexplored avenues for plant improvement[47]. Third, the sucrose ferulate cycle establishes a new metabolic paradigm for ferulate unit incorporation into the cell wall matrix with applications in synthetic biology of complex polymers.

Methods

Plant materials and chemicals

The *dow1-1* and *dow1-2* mutants were isolated from the UniformMu population by introgressing the *Mu* active line into the inbred W22 genetic background as described previously[48]. Plants were grown under natural conditions in the Shandong University Experiment Station. FA was purchased from Sigma-Aldrich, Fer-CoA and [$^2H_3$]FA from Shanghai ZZBIO, sibiricose A5 and cinnamic acid from Shanghai Yuanye Bio-Technology, and CoA from Sangon Biotech.

Transmission electron microscopy analysis

The wild-type and *dow1-1* embryos at 15 DAP were fixed with fixative solution (4% paraformaldehyde, 0.1 M PBS (0.162 M Na_2HPO_4, 0.038 M NaH_2PO_4, pH 7.4), 2.5% glutaraldehyde). The samples were washed five or six times with 0.1 M PBS on ice; dehydrated on ice with an ethanol gradient twice; soaked in 1/3, 1/2 and 2/3 LR White resin (medium acrylic resin, London Resin Company) and pure LR White resin for 24 hours each time at room temperature; and polymerized at 45 °C for one day, 55 °C for two days and 60 °C for one day. After polymerization, the samples were cut into 100 nm sections. The slices were stained by uranyl acetate and lead citrate and observed under a transmission electron microscope (Thermo Scientific, FEI Tecnai G2 F20).

Analysis of esterified phenolic acids in maize cell walls

The cell-wall-bound phenolic acids were extracted from freeze-dried embryos, endosperm and roots and analysed using the method described previously with some modifications[36]. Endosperm (100 mg), embryo (20 mg) or root (5 mg) samples were extracted with 1 ml of 80:20 ethanol:water (v:v). The suspensions were vortexed until all the samples were suspended, sonicated for 10 min, heated to 80 °C

for 15 min and then centrifuged for 15 min at 5,000*g*, and the supernatant was discarded. The samples were then extracted two further times with sonication but no heating. A 3 µl internal standard (cinnamic acid at 2 mg ml^{-1}) was added to the wet pellet, and the samples were hydrolysed by suspension in 0.8 ml of 2 M NaOH for 16 h in the dark. After centrifugation for 15 min at 5,000*g*, the supernatant was acidified to pH 2 by the addition of 220 µl of 12 M HCl. Bound phenolic acids were extracted into ethyl acetate (1 × 500 µl, 1 × 500 µl, 1 × 500 µl and 1 × 500 µl) by vortexing and centrifugation at 14,000*g* for 5 min. After evaporation by high-purity nitrogen, bound phenolic acids were dissolved in 100 µl of 2% acetic acid and centrifuged for 10 min. HPLC separation of the supernatant was carried out using a reverse-phase C18 column (4.6 × 250 mm, 5 µm, Agilent ZORBAX SB-C18) at 40 °C and a Shimadzu LC-20AT HPLC equipped with a diode array detector SPD-M20A. 20 µl of each sample was loaded and analysed using absorption between 190 and 600 nm. A gradient of solvent A (0.2% TFA) and solvent B (acetonitrile) at a flow rate of 1 ml min^{-1} was used as previously described[33]: 0–5 min, 10% B isocratic; 5–25 min, 10–30% B linear; 25–40 min, 30% B isocratic; 40–45 min, 30–35% B linear; 45–46 min, 35–100% B linear; 46–51 min, 100% B isocratic; 51–53 min, 100–10% B linear; and 53–60 min, 10% B isocratic. Statistical analysis was done using GraphPad Prism (version 9.0.2).

Anhydrous mild acidolysis

The cell wall HCA conjugates were extracted from 20 mg of freeze-dried embryos or 50 mg of endosperm and analysed using the method described previously[37] with some modifications. Endosperm or embryo samples were extracted with 1 ml of 80:20 (v:v) ethanol:water. The suspensions were vortexed until all the samples were suspended, sonicated for 10 min, heated to 80 °C for 15 min and then centrifuged for 15 min at 5,000*g*, and the supernatant was discarded. The samples were then extracted two further times with sonication but no heating and 1 ml of absolute ethanol. The samples were oven-dried at 55 °C and then mixed into 500 µl of a dry acidolysis reagent. This reagent was prepared by carefully adding 0.7 ml of acetyl chloride to 20 ml of 70/30 (v/v) dioxane/absolute methanol. The samples were heated at 80 °C for 3 h at 750 rpm. After the reaction, 3 µl of 0.2 mg ml^{-1} coumaric acid was added as an internal standard. Then, 500 µl of water was added, and the mixture was extracted with four portions of ethyl acetate. The organic layers were combined and dried by high-purity nitrogen. The residue was dissolved in 100 µl of acetonitrile and centrifuged before HPLC analysis. HPLC separation was carried out using a reverse-phase C18 column (4.6 × 250 mm, 5 µm, Agilent ZORBAX SB-C18) at 40 °C and a Shimadzu LC-20AT HPLC equipped with a diode array detector SPD-M20A. 20 µl of each sample was loaded and analysed using absorption between 190 and 600 nm. A gradient of solvent A (0.1% TFA) and solvent B (acetonitrile) at a flow rate of 1 ml min^{-1} was used: 0–2 min, 10% B isocratic; 2–6.5 min, 10–18% B linear; 6.5–21 min, 18–50% B linear; 21–22 min, 50% B isocratic; 22–23 min, 50–100% B linear; 23–33 min, 100% B isocratic; 33–34 min, 100–10% B linear; and 34–40 min, 10% B isocratic. The peak area ratios (*p*CA-Ara/IS and FA-Ara/IS; IS denotes internal standard) at 325 nm (*p*CA-Ara and FA-Ara) and 280 nm (IS) were used to compare the proportion of HCA conjugates among samples. Statistical analysis was done using GraphPad Prism (version 9.0.2).

TFA mild acidolysis

The cell wall HCA conjugates were extracted and analysed using the method described previously with some modifications[31]. Root (5 mg) samples were extracted with 1 ml of 80:20 ethanol:water. The suspensions were vortexed until all the samples were suspended, sonicated for 10 min, heated to 80 °C for 15 min and then centrifuged for 15 min at 5,000*g*, and the supernatant was discarded. The samples were then extracted two further times with sonication but no heating. The samples were treated with 1.2 ml 50 mM TFA for 4 h at 99 °C with agitation at 750 rpm. After centrifugation for 10 min at 16,000*g*, 1 ml of supernatant was freeze-dried. Released HCA conjugates from the supernatant were dissolved in 300 µl of 50% acetonitrile for LC–MS/MS analysis.

Analysis of the methanol extracts from maize seeds

To investigate the water- and alcohol-soluble compounds in the *dow1* mutant, the embryos and endosperms of the wild-type and *dow1-1* were extracted by 90% methanol and analysed by HPLC. 20 mg of embryos at 15 DAP were ground and extracted with 500 µl of 90% methanol. 100 mg of ground endosperm was extracted with 1 ml of 90% methanol. For each sample, an internal standard of 0.08 mM cinnamic acid was added during extraction. The extraction was carried out at 4 °C for 12 h with a slow rotation. After centrifugation at 16,000*g* for 10 min at room temperature, the supernatant was analysed by HPLC as in the analysis of cell wall esterified phenolic acids except for the gradient composition. The gradient elution with solvent A (1‰ TFA) and solvent B (acetonitrile) was 0–2 min, 10% B isocratic; 2–32 min, 10–35% B linear; 32–33 min, 35-100% B linear; 33–43 min, 100% B isocratic; 43–44 min, 100–10% B linear; and 44–50 min, 10% B isocratic. The supernatant of *dow1-1* embryo extract was blown dry with pure nitrogen and dissolved in 150 µl of sterile water for enzyme activity analysis.

Preparation of the CMF

Maize seeds were ground into powder in liquid nitrogen, extracted with extraction buffer (0.4 M sucrose, 50 mM MOPs, 1 mM EDTA, 1 mM DTT) and then filtered with two layers of Miracloth. The extract was centrifuged at 47,810*g* (Sorvall ss-34 rotor, Thermo Scientific) for 15 min at 4 °C. The supernatant was carefully removed and re-centrifuged at 100,000*g* (Type 70Ti rotor, Beckman Coulter) for 1 h at 4 °C. The pellet was suspended in 100 mM K-phosphate buffer as the CMF, and the protein concentration was determined by the Bradford method.

Enzyme activity assays

For reactions with the CMF and *dow1-1* embryo extract, the reaction mixture contained 60 mM K-phosphate buffer (30 mM K_2HPO_4, 60 mM KH_2PO_4, pH 6.0), 2.5 mM $MgCl_2$, 1 mM $CoCl_2$, 10 µg MBP–DOW1, 250 µM Fer-CoA, 200 µg wild-type seed CMF, 50 µl *dow1-1* embryo extract and sterile water to make up the mixture to 150 µl. The reaction was incubated at 30 °C for 24 h and then stopped by adding 50 µl of 0.2 M acetic acid and boiling at 100 °C for 5 min. After centrifugation at 16,000*g* for 5 min at room temperature, the supernatant was analysed by HPLC. HPLC was carried out similarly to the analysis of the 90% methanol extracts of embryos. For the DOW1 in vitro enzyme activity, the reaction mixture contained 50 mM K-phosphate buffer (25 mM K_2HPO_4, 50 mM KH_2PO_4, pH 6.0), 2.5 mM $MgCl_2$, 1 mM $CoCl_2$, 10 µg MBP–DOW1 or MBP, 500 µM Fer-CoA, 500 µM sibiricose A5 and sterile water to make up the mixture to 100 µl. The reaction was incubated at 30 °C for 5 h. The reaction was stopped and analysed in the same way as indicated above. For SFT1, SFT2, SFT3 and SFT4 in vitro enzyme activity, the reaction mixture contained 40 mM K-phosphate buffer (20 mM K_2HPO_4, 40 mM KH_2PO_4, pH 6.0), 2.5 mM $MgCl_2$, 1 mM $CoCl_2$, 10 µg MBP–SFT1/SFT2/SFT3/SFT4 or MBP, 250 µM Fer-CoA, 1 mM sucrose and sterile water to make up the mixture to 100 µl. The reaction was incubated at 30 °C for 5 h, stopped and analysed similarly. The kinetics of DOW1, SFT1, SFT2, SFT3 and SFT4 were determined by quantification of the reactive products with a gradient amount of the above substrates. The K_m constant was calculated by fitting the initial velocities to the Michaelis–Menten equation.

Large-scale preparation of Peak 2

The methanol extract from the *dow1-1* mutant seeds was used as the substrate of MBP–DOW1 in the preparation of Peak 2. The *dow1-1* seeds at 15 DAP were freeze-dried and ground into a fine powder. 80 g of the powder was spin-extracted with 500 ml of 90% methanol at 4 °C overnight. The extract was centrifuged at 16,000*g* for 10 min at room temperature, and the supernatant was evaporated to dry by

vacuum rotary evaporation, dissolved in 120 ml of sterile water and stored at −80 °C.

The preparation reaction occurred in a 306 ml mixture, which contained 25 ml of 200 mM K-phosphate buffer (100 mM K_2HPO_4, 200 mM KH_2PO_4, pH 6.0), 10 ml of 50 mM $MgCl_2$, 2 ml of 100 mM $CoCl_2$, 5.76 mg of MBP–DOW1, 20 mg of Fer-CoA, 100 ml of *dow1-1* embryo extract and 100 mM K-phosphate buffer to make up to 306 ml. The reaction was carried out at 30 °C for 24 h and stopped by adding 102 ml of 0.2 M acetic acid and then boiling at 100 °C for 5 min. The mixture was centrifuged at 16,000*g* for 10 min at room temperature. The supernatant was freeze-dried and dissolved in 12 ml of 30% acetonitrile (HPLC grade). The solution was centrifuged at 3,000*g* for 5 min at room temperature. The upper organic phase was collected and applied to preparation for HPLC using a reverse-phase C18 column (HiQSil, 10 mm) and a Shimadzu LC-6AD semi-preparative LC system. Each injection was 80 µl and analysed at 325 nm absorption. A binary gradient elution method with solvent A (pure water) and solvent B (acetonitrile) at a flow rate of 4 ml min^{-1} was used. The gradient elution condition was 0–2 min, 15% B isocratic; 2–17 min, 15–30% B linear; 17–27 min, 30% B isocratic; 27–40 min, 30–40% B linear; 40–41 min, 40–100% B linear; 41–51 min, 100% B isocratic; 51–52 min, 100–15% B linear; and 52–60 min, 15% B isocratic. Peak 2 was collected between 22 min and 23.5 min. A total of 240 ml of collected Peak 2 was concentrated using a vacuum rotary evaporator to about 45 ml before being freeze-dried. Purified Peak 2 showed high purity in the HPLC analysis (Supplementary Fig. 5f, trace 2). The minor peaks in a small amount were proved to be Peak 2 isomers (Supplementary Fig. 5f, trace 2).

Chemical structure determination of Peak 2

The chemical structure of Peak 2 was determined by HPLC–HR-MS/MS (Supplementary Fig. 2) and NMR analysis (Supplementary Figs. 5a–e and 6 and Supplementary Table 1). Peak 2 (5 mg) was dissolved in CD_3OD and analysed by NMR. NMR spectra were recorded on a Bruker Avance III 600 MHz spectrometer, and NMR data were processed by using MestReNova. Peak 2 is 2-*O*-α-D-glucopyranosyl-(1′→2)-3,6-*O*-feruloyl-β-D-fructofuranoside—that is, 3,6-*O*-diferuloyl sucrose (3,6-*O*-diFer sucrose). ^{1}H NMR (600 MHz, CD_3OD) (δ in ppm, *J* in Hz) δ7.71 (*d*, *J* = 15.9 Hz, 1H), 7.65 (*d*, *J* = 15.9 Hz, 1H), 7.23 (*d*, *J* = 1.8 Hz, 1H), 7.19 (*d*, *J* = 1.8 Hz, 1H), 7.13 (*dd*, *J* = 8.2, 1.9 Hz, 1H), 7.09 (*dd*, *J* = 8.2, 1.8 Hz, 1H), 6.81 (*d*, *J* = 0.6 Hz, 1H), 6.80 (*d*, *J* = 0.9 Hz, 1H), 6.43 (*d*, *J* = 15.9 Hz, 1H), 6.40 (*d*, *J* = 15.9 Hz, 1H), 5.48 (*d*, *J* = 7.8 Hz, 1H), 5.44 (*d*, *J* = 3.7 Hz, 1H), 4.55 (*dd*, *J* = 11.8, 7.3 Hz, 1H), 4.50 (*dd*, *J* = 11.8, 3.7 Hz, 1H), 4.44 (*t*, *J* = 7.8 Hz, 1H), 4.16 (*td*, *J* = 7.5, 3.7 Hz, 1H), 3.98–3.94 (*m*, 1H), 3.92 (*m*, 1H), 3.90 (*s*, 3H), 3.89 (*s*, 3H), 3.88 (*m*, 1H), 3.87 (*m*, 1H), 3.79 (*dd*, *J* = 11.9, 4.6 Hz, 1H), 3.68–3.63 (*m*, 2H), 3.61–3.57 (*m*, 1H), 3.44–3.37 (*m*, 2H). ^{13}C NMR (151 MHz, CD_3OD) δ 169.03, 168.25, 150.74 (overlapped), 147.79, 147.23, 127.71, 127.68, 124.23 (overlapped), 116.50, 116.48, 115.17, 115.00, 112.11, 111.71, 105.12, 93.13, 81.30, 79.27, 75.01, 75.00, 74.41, 73.24, 71.48, 66.21, 65.19, 62.68, 56.52, 56.48.

Treatment of plants

On the basis of the UV absorption, the 6-[$^2H_3$]P2, 3-[$^2H_3$]P2 and [$^2H_3$]FA solutions were adjusted to equimolar (Extended Data Fig. 3d). In a separate experiment, 6-[$^2H_3$]P3 and [$^2H_3$]FA were adjusted to equimolar in the feeding experiment (Extended Data Fig. 3e). Eight W22 embryos at 18 to 20 DAP were placed in Petri dishes with 30 ml of Murashige and Skoog medium containing 13.9 µM 6-[$^2H_3$]P2, 3-[$^2H_3$]P2 and [$^2H_3$]FA and 27.8 µM [$^2H_3$]FA. 13.9 µM methanol was used as a control. In the 6-[$^2H_3$]P3 feeding test, 6.95 µM 6-[$^2H_3$]P3 and 6.95 µM [$^2H_3$]FA in 30 ml of Murashige and Skoog medium were used. The embryos were cultivated in the dark at 30 °C for 4 days and then in a light incubator at 22 °C for 17 days (6-[$^2H_3$]P2 and 3-[$^2H_3$]P2 treatment groups and control) or for 13 days (6-[$^2H_3$]P3 treatment group and control). The seedlings were rinsed thoroughly with water and then sterile water. The roots of the seedlings were ground into a powder with liquid nitrogen and freeze-dried. The cell wall esterified FA of 5 mg of freeze-dried root was extracted and dissolved in 100 µl of 2% acetic acid. [$^2H_3$]FA was detected using HPLC–HR Q-TOF MS (HPLC–HR-MS, Bruker). The mass spectrometer operated in an ESI-negative mode.

The cell wall esterified FA was predominantly FA monomer but also a small amount of diFA. There are many types of diFAs (Extended Data Fig. 10a), as described previously[42]. Most types of dimers are non-decarboxylated with the chemical formula $C_{20}H_{18}O_8$. The decarboxylated dimer has the chemical formula $C_{19}H_{18}O_6$. The chemical formula of FA monomer is $C_{10}H_{10}O_4$, and the calculated *m/z* of $[M\text{-}H]^-$ is 193.0495. The chemical formula of [$^2H_3$]FA monomer is $C_{10}H_7D_3O_4$, and the calculated *m/z* of $[M\text{-}H]^-$ is 196.0684. The chemical formula of single FA-labelled non-decarboxylated FA dimer ($^2H_3$-non-decarboxylated diFA) is $C_{20}H_{15}D_3O_8$, and the calculated *m/z* of $[M\text{-}H]^-$ is 388.1106. The chemical formula of double FA-labelled non-decarboxylated FA dimer ($^2H_6$-non-decarboxylated diFA) is $C_{20}H_{12}D_6O_8$, and the calculated *m/z* of $[M\text{-}H]^-$ is 391.1295. The chemical formula of single FA-labelled decarboxylated FA dimer ($^2H_3$-decarboxylated diFA) is $C_{19}H_{15}D_3O_6$, and the calculated *m/z* of $[M\text{-}H]^-$ is 344.1208. The chemical formula of double FA-labelled decarboxylated FA dimer ($^2H_6$-decarboxylated diFA) is $C_{19}H_{12}D_6O_6$, and the calculated *m/z* of $[M\text{-}H]^-$ is 347.1396.

HPLC–HR-MS and HPLC–HR-MS/MS

HPLC–HR–MS/MS was performed on a rapid-separation LC system (Dionex, UltiMate3000, UHPLC) coupled with an ESI-Q-TOF mass spectrometer (Bruker Daltonics, Impact HD). HPLC separation was carried out using a reverse-phase C18 column (4.6 × 250 mm, 5 µm, Agilent ZORBAX SB-C18) at 40 °C with a mobile phase system of 0.1% formic acid (Sigma) in Mili-Q filtered water (A) and 0.1% formic acid (Sigma) in acetonitrile (Fisher Scientific) (B). For HPLC–HR-MS analysis of cell wall esterified [$^2H_3$]FA, a gradient of solvent A and solvent B at a flow rate of 1 ml min^{-1} was used for the analysis of esterified phenolic acids in maize cell walls. For HPLC–HR-MS of 6-[$^2H_3$]P2, 3-[$^2H_3$]P2, 6-[$^2H_3$]P3, Peak A and Peak B and for HPLC–HR-MS/MS of Peak 1, Peak 2 and Peak 3, the gradient elution method with solvent A and solvent B at a flow rate of 1 ml min^{-1} was used in the analysis of the methanol extracts from maize seeds. Each sample loaded 20 µl was analysed using absorption between 190 and 400 nm.

The MS (MS/MS) analysis was performed using OtofControl (Bruker Daltonics) under the following conditions: ESI-negative mode for scanning, ESI capillary voltage with 4.5 kV, Quadratic+HPC mode for internal mass calibration, nebulizer gas nitrogen with 0.5 bar, dry gas nitrogen with 6 l min^{-1}, probe temperature of 200 °C and full scan mass range from 50 to 1,500 *m/z*. The precursor ions intensity threshold greater than 3.0×10^3 in the quadrupole was selected for auto MS/MS fragmentation analysis. The exclusion was used after three spectra within 60 s. The mass correction solution was 10 mM HCOONa. HCOONa was dissolved in 50% isopropyl alcohol (isopropyl alcohol:H_2O = 1:1(v/v)). The data were analysed using Data Analysis software (Bruker Daltonics).

Reporting summary

Further information on research design is available in the Nature Portfolio Reporting Summary linked to this article.

Data availability

All data are available in this article and its extended data figures and supplementary figures and tables. Source data are provided with this paper.

References

1. Sabbadin, F. et al. Secreted pectin monooxygenases drive plant infection by pathogenic oomycetes. *Science* **373**, 774–779 (2021).
2. Zhang, Y. et al. Molecular insights into the complex mechanics of plant epidermal cell walls. *Science* **372**, 706–711 (2021).

3. Liu, C., Yu, H., Voxeur, A., Rao, X. & Dixon, R. A. FERONIA and wall-associated kinases coordinate defense induced by lignin modification in plant cell walls. *Sci. Adv.* **9**, eadf7714 (2023).
4. Carpita, N. C. Structure and biogenesis of the cell walls of grasses. *Annu. Rev. Plant Physiol. Plant Mol. Biol.* **47**, 445–476 (1996).
5. Fry, S. C. Cross-linking of matrix polymers in the growing cell walls of angiosperms. *Ann. Rev. Plant Physiol.* **37**, 165–186 (1986).
6. Grabber, J. H., Ralph, J. & Hatfield, R. D. Cross-linking of maize walls by ferulate dimerization and incorporation into lignin. *J. Agric. Food Chem.* **48**, 6106–6113 (2000).
7. Feijao, C. et al. Hydroxycinnamic acid-modified xylan side chains and their cross-linking products in rice cell walls are reduced in the *Xylosyl arabinosyl substitution of xylan 1* mutant. *Plant J.* **109**, 1152–1167 (2021).
8. Varner, J. E. & Lin, L. S. Plant cell wall architecture. *Cell* **56**, 231–239 (1989).
9. Zhong, R., Cui, D. & Ye, Z. H. Secondary cell wall biosynthesis. *N. Phytol.* **221**, 1703–1723 (2019).
10. Gao, Y., Lipton, A. S., Wittmer, Y., Murray, D. T. & Mortimer, J. C. A grass-specific cellulose–xylan interaction dominates in sorghum secondary cell walls. *Nat. Commun.* **11**, 6081 (2020).
11. Kang, X. et al. Lignin–polysaccharide interactions in plant secondary cell walls revealed by solid-state NMR. *Nat. Commun.* **10**, 347 (2019).
12. Simmons, T. J. et al. Folding of xylan onto cellulose fibrils in plant cell walls revealed by solid-state NMR. *Nat. Commun.* **7**, 13902 (2016).
13. Scheller, H. V. & Ulvskov, P. Hemicelluloses. *Annu. Rev. Plant Biol.* **61**, 263–289 (2010).
14. Hatfield, R. D., Rancour, D. M. & Marita, J. M. Grass cell walls: a story of cross-linking. *Front. Plant Sci.* **7**, 2056 (2016).
15. Terrett, O. M. & Dupree, P. Covalent interactions between lignin and hemicelluloses in plant secondary cell walls. *Curr. Opin. Biotechnol.* **56**, 97–104 (2019).
16. Waterstraat, M. & Bunzel, M. A multi-step chromatographic approach to purify radically generated ferulate oligomers reveals naturally occurring 5-5/8-8(cyclic)-, 8-8(noncyclic)/8-*O*-4-, and 5-5/8-8(noncyclic)-coupled dehydrotriferulic acids. *Front. Chem.* **6**, 190 (2018).
17. Bento-Silva, A., Vaz Patto, M. C. & do Rosário Bronze, M. Relevance, structure and analysis of ferulic acid in maize cell walls. *Food Chem.* **246**, 360–378 (2018).
18. Ralph, J., Quideau, S., Grabber, J. H. & Hatfield, R. D. Identification and synthesis of new ferulic acid dehydrodimers present in grass cell walls. *J. Chem. Soc. Perkin 1* **23**, 3485–3498 (1994).
19. Buanafina, M. M. d. O. Feruloylation in grasses: current and future perspectives. *Mol. Plant* **2**, 861–872 (2009).
20. Bily, A. C. et al. Dehydrodimers of ferulic acid in maize grain pericarp and aleurone: resistance factors to *Fusarium graminearum*. *Phytopathology* **93**, 712–719 (2003).
21. Mnich, E. et al. Phenolic cross-links: building and de-constructing the plant cell wall. *Nat. Prod. Rep.* **37**, 919–961 (2020).
22. Wilkerson, C. G. et al. Monolignol ferulate transferase introduces chemically labile linkages into the lignin backbone. *Science* **344**, 90–93 (2014).
23. Lynd, L. R. et al. How biotech can transform biofuels. *Nat. Biotechnol.* **26**, 169–172 (2008).
24. Fry, S. C., Willis, S. C. & Paterson, A. E. Intraprotoplasmic and wall-localised formation of arabinoxylan-bound diferulates and larger ferulate coupling-products in maize cell-suspension cultures. *Planta* **211**, 679–692 (2000).
25. Myton, K. E. & Fry, S. C. Intraprotoplasmic feruloylation of arabinoxylans in *Festuca arundinacea* cell cultures. *Planta* **193**, 326–330 (1994).
26. Yoshida-Shimokawa, T., Yoshida, S., Kakegawa, K. & Ishii, T. Enzymic feruloylation of arabinoxylan-trisaccharide by feruloyl-CoA: arabinoxylan-trisaccharide *O*-hydroxycinnamoyl transferase from *Oryza sativa*. *Planta* **212**, 470–474 (2001).
27. Mitchell, R. A., Dupree, P. & Shewry, P. R. A novel bioinformatics approach identifies candidate genes for the synthesis and feruloylation of arabinoxylan. *Plant Physiol.* **144**, 43–53 (2007).
28. Moghe, G. et al. BAHD company: the ever-expanding roles of the BAHD acyltransferase gene family in plants. *Annu. Rev. Plant Biol.* **74**, 165–194 (2023).
29. Buanafina, M. Md. O., Fescemyer, H. W., Sharma, M. & Shearer, E. A. Functional testing of a PF02458 homologue of putative rice arabinoxylan feruloyl transferase genes in *Brachypodium distachyon*. *Planta* **243**, 659–674 (2016).
30. Molinari, H. B., Pellny, T. K., Freeman, J., Shewry, P. R. & Mitchell, R. A. Grass cell wall feruloylation: distribution of bound ferulate and candidate gene expression in *Brachypodium distachyon*. *Front. Plant Sci.* **4**, 50 (2013).
31. Souza, W. R. et al. Suppression of a single BAHD gene in *Setaria viridis* causes large, stable decreases in cell wall feruloylation and increases biomass digestibility. *N. Phytol.* **218**, 81–93 (2018).
32. Piston, F. et al. Down-regulation of four putative arabinoxylan feruloyl transferase genes from family PF02458 reduces ester-linked ferulate content in rice cell walls. *Planta* **231**, 677–691 (2010).
33. Chiniquy, D. et al. XAX1 from glycosyltransferase family 61 mediates xylosyltransfer to rice xylan. *Proc. Natl Acad. Sci. USA* **109**, 17117–17122 (2012).
34. Bartley, L. E. et al. Overexpression of a BAHD acyltransferase, Os*At10*, alters rice cell wall hydroxycinnamic acid content and saccharification. *Plant Physiol.* **161**, 1615–1633 (2013).
35. Mota, T. A.-O. et al. Suppression of a BAHD acyltransferase decreases *p*-coumaroyl on arabinoxylan and improves biomass digestibility in the model grass *Setaria viridis*. *Plant J.* **105**, 136–150 (2021).
36. Pellny, T. K. et al. Cell walls of developing wheat starchy endosperm: comparison of composition and RNA-seq transcriptome. *Plant Physiol.* **158**, 612–627 (2012).
37. Eugene, A., Lapierre, C. & Ralph, J. Improved analysis of arabinoxylan-bound hydroxycinnamate conjugates in grass cell walls. *Biotechnol. Biofuels* **13**, 202 (2020).
38. Tan, B. C., Schwartz, S. H., Zeevaart, J. A. & McCarty, D. R. Genetic control of abscisic acid biosynthesis in maize. *Proc. Natl Acad. Sci. USA* **94**, 12235–12240 (1997).
39. Withers, S. et al. Identification of grass-specific enzyme that acylates monolignols with *p*-coumarate. *J. Biol. Chem.* **287**, 8347–8355 (2012).
40. Petrik, D. L. et al. *p*-Coumaroyl-CoA:monolignol transferase (PMT) acts specifically in the lignin biosynthetic pathway in *Brachypodium distachyon*. *Plant J.* **77**, 713–726 (2014).
41. Sibout, R. et al. Structural redesigning *Arabidopsis* lignins into alkali-soluble lignins through the expression of *p*-coumaroyl-CoA:monolignol transferase PMT. *Plant Physiol.* **170**, 1358–1366 (2016).
42. Nakano, K., Murakami, K., Takaishi, Y. & Tomimatsu, T. Feruloyl sucrose derivatives from *Heloniopsis orientalis*. *Chem. Pharm. Bull.* **34**, 5005–5010 (1986).
43. Yan, L., Gao, W., Zhang, Y. & Wang, Y. A new phenylpropanoid glycosides from *Paris polyphylla* var. *yunnanensis*. *Fitoterapia* **79**, 306–307 (2008).
44. Cha, J.-G. et al. Feruloyl sucrose esters from *Oryza sativa* roots and their Tyrosinase inhibition activity. *Chem. Nat. Compd.* **51**, 1094–1098 (2015).

45. Chen, X.-Y., Wang, R.-F. & Liu, B. An update on oligosaccharides and their esters from traditional Chinese medicines: chemical structures and biological activities. *Evid. Based Complement. Alternat. Med.* **2015**, 512675–512697 (2015).
46. Hatfield, R. D., Jung, H., Marita, J. M. & Kim, H. Cell wall characteristics of a maize mutant selected for decreased ferulates. *Am. J. Plant Sci.* **9**, 446–466 (2018).
47. Penning, B. W., McCann, M. C. & Carpita, N. C. Evolution of the cell wall gene families of grasses. *Front. Plant Sci.* **10**, 1205 (2019).
48. McCarty, D. R. et al. Steady-state transposon mutagenesis in inbred maize. *Plant J.* **44**, 52–61 (2005).

Acknowledgements

We thank T. Beuerle for the gift of recombinant plasmid 4CL/pCRT7 for the prokaryotic expression of 4Cl and S. Cao and M. Hou for assistance in RT–qPCR, confocal and DNA blotting experiments. This research was supported by the National Natural Science Foundation of China (project no. 32230075, B.-C.T.).

Author contributions

D.Y. and B.-C.T. conceived and designed the experiments. D.Y. performed most of the experiments. X.L., Y.Z. and H.Y. cloned *Dow1*. X.Z., M.L. and S.L. analysed the NMR data, and X.Z. contributed to experimental discussions. H.L. performed the prokaryotic expression of SFT1 to SFT4. D.Y. and B.-C.T. analysed the data and wrote the paper. K.E.K. and D.R.M. revised the paper.

Competing interests

The authors declare no competing interests.

Additional information

Extended data is available for this paper at https://doi.org/10.1038/s41477-024-01781-1.

Supplementary information The online version contains supplementary material available at https://doi.org/10.1038/s41477-024-01781-1.

Correspondence and requests for materials should be addressed to Bao-Cai Tan.

Peer review information *Nature Plants* thanks the anonymous reviewers for their contribution to the peer review of this work.

Reprints and permissions information is available at www.nature.com/reprints.

Publisher's note Springer Nature remains neutral with regard to jurisdictional claims in published maps and institutional affiliations.

Dalin Yang[1], Hui Liu[1], Xiaojie Li[2], Yafeng Zhang[3], Xingwang Zhang[4], Huanhuan Yang[5], Mingyu Liu[4], Karen E. Koch[6], Donald R. McCarty[6], Shengying Li[4] & Bao-Cai Tan[1]

[1]Key Laboratory of Plant Development and Environmental Adaptation Biology, Ministry of Education, School of Life Science, Shandong University, Qingdao, China. [2]Agricultural Genomics Institute at Shenzhen, Chinese Academy of Agricultural Sciences, Shenzhen, China. [3]Guangdong Provincial Key Laboratory of Plant Molecular Breeding, College of Agriculture, South China Agricultural University, Guangzhou, China. [4]State Key Laboratory of Microbial Technology, Shandong University, Qingdao, China. [5]School of Life Sciences, Qilu Normal University, Jinan, China. [6]Hoirticultural Sciences Department, University of Florida, Gainesville, FL, USA. e-mail: bctan@sdu.edu.cn

https://doi.org/10.1038/s41477-024-01781-1

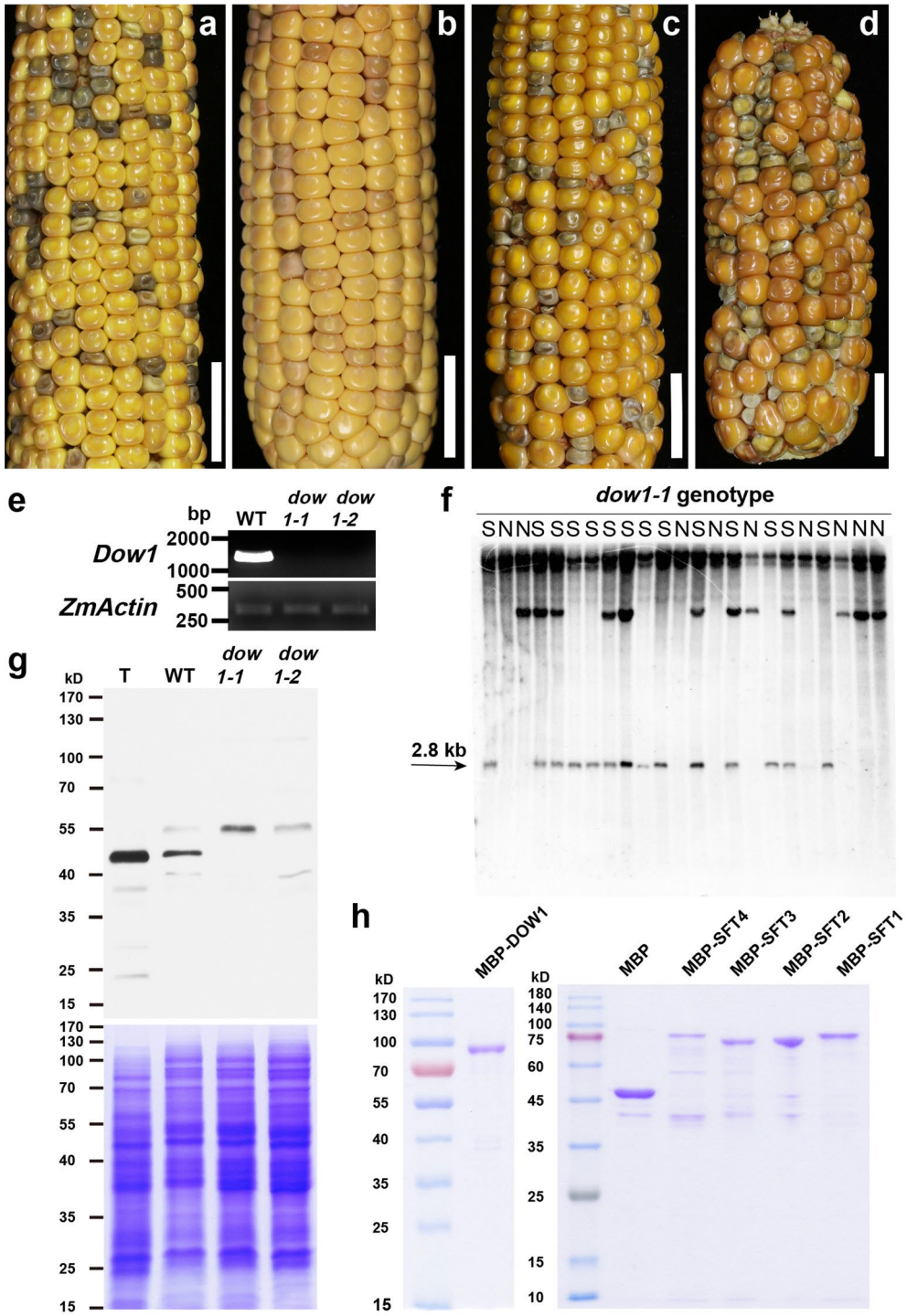

Extended Data Fig. 1 | Genetic verification of Dow1 and proteins prokaryotic expression. a, **b**, 18 DAP ears segregating for the *dow1-1* (**a**) and *dow1-2* (**b**) mutation, respectively. **c**, *dow1-1*/*dow1-2* ear. **d**, *dow1-2*/*dow1-1* ear; Bar=2 cm in (**a**), (**b**), (**c**), and (**d**). **e**, RT-PCR analysis of *Dow1* expression in the *dow1* mutants. Total RNA was isolated from the *dow1* mutants and WT embryos at 15 DAP, reverse-transcribed, and used as templates in the RT-PCR analysis. **f**, Southern blot analysis identified a 2.8 kb *Spe* I fragment carrying a *Mu*8 insertion linked to the *Dow1* mutation. DNAs from a segregating F2 population of *dow1-1* were digested with *Spe* I, blotted, and hybridized with a *Mu*8-specific probe. N, non-segregating (WT); S, segregating (heterozygous). **g**, Specificity of DOW1 antibody. T: total proteins from 7-day-old seedlings; WT: total proteins from 15 DAP WT embryos; *dow1-1* and *dow1-2*: total proteins from 15 DAP *dow1-1* and *dow1-2* embryos. For each sample, 60 μg total protein was loaded. **h**, MBP-DOW1, MBP-SFT1, MBP-SFT2, MBP-SFT3, MBP-SFT4, and MBP prokaryotic expression. For each protein, 2 μg protein was loaded. MBP-DOW1: 90 kD; MBP-SFT1: 91 kD; MBP-SFT2: 91 kD; MBP-SFT3: 91 kD; MBP-SFT4: 90; MBP: 44 kD. Experiments were repeated independently with similar results at least 3 times (**e**-**h**).

https://doi.org/10.1038/s41477-024-01781-1

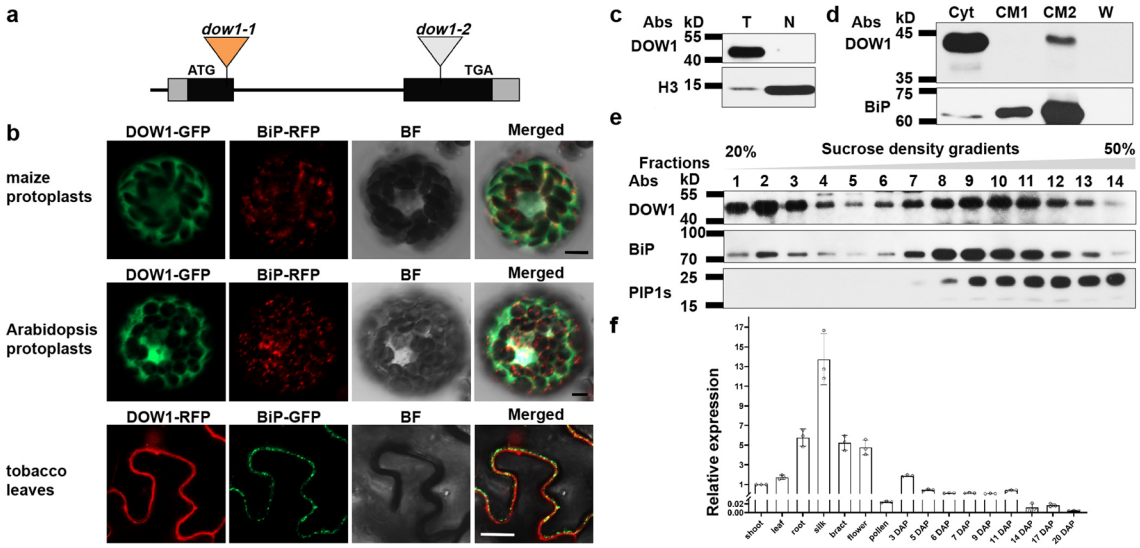

Extended Data Fig. 2 | Dow1 encodes a BAHD acyltransferase protein localized in the cytosol and membrane. a, Gene structure of *Dow1* and locations of the *Mu* insertions in two independent alleles. Exons are closed boxes, and introns are lines. **b**, Co-transfecting the maize protoplasts, Arabidopsis protoplasts, and tobacco leaves with GFP-fused DOW1 and RFP-fused BiP, GFP-fused DOW1 and RFP-fused BiP, RFP-fused DOW1 and GFP-fused BiP. Scale bar=5 μm for maize protoplasts, 5 μm for Arabidopsis protoplasts, and 20 μm for tobacco leaves. BiP-RFP was used to indicate endoplasmic reticulum (ER). BF, bright field. **c**, Immunoblot analysis of total proteins and nucleus proteins. DOW1 does not accumulate in the nucleus. Anti-H3 was used to indicate the nucleus. T: total proteins from 3-day-old seedlings; N: nuclear protein. **d**, Immunoblot analysis of cytoplasm non-membranous proteins and cell total membranous proteins. Cyt: Cytoplasm non-membranous proteins; CM1: cell total membranous proteins; CM2: 5 times the concentration of CM1; W: supernatant of washing cell total membranous proteins; Anti-BiP was used to indicate ER. Abs, antibodies. **e**, Immunoblot analysis of the fractions obtained from maize seedlings by a sucrose density gradient centrifugation. The distribution pattern of DOW1 is identical to that of BiP, which is an ER marker, indicating that DOW1 is localized to ER. Anti-BiP and anti-PIP1s antibodies were used to indicate ER and plasma membrane. Abs, antibodies. **f**, RT-qPCR analysis of the *Dow1* transcript levels in major maize tissues. Error bars=mean ± SD (n = 3 replicates of assays with independent samples). Total RNA was isolated from all tissues, reverse-transcribed, and used as templates. Kernels are indicated as DAP (days after pollination). Experiments were repeated independently with similar results at least 3 times (**b**-**e**).

https://doi.org/10.1038/s41477-024-01781-1

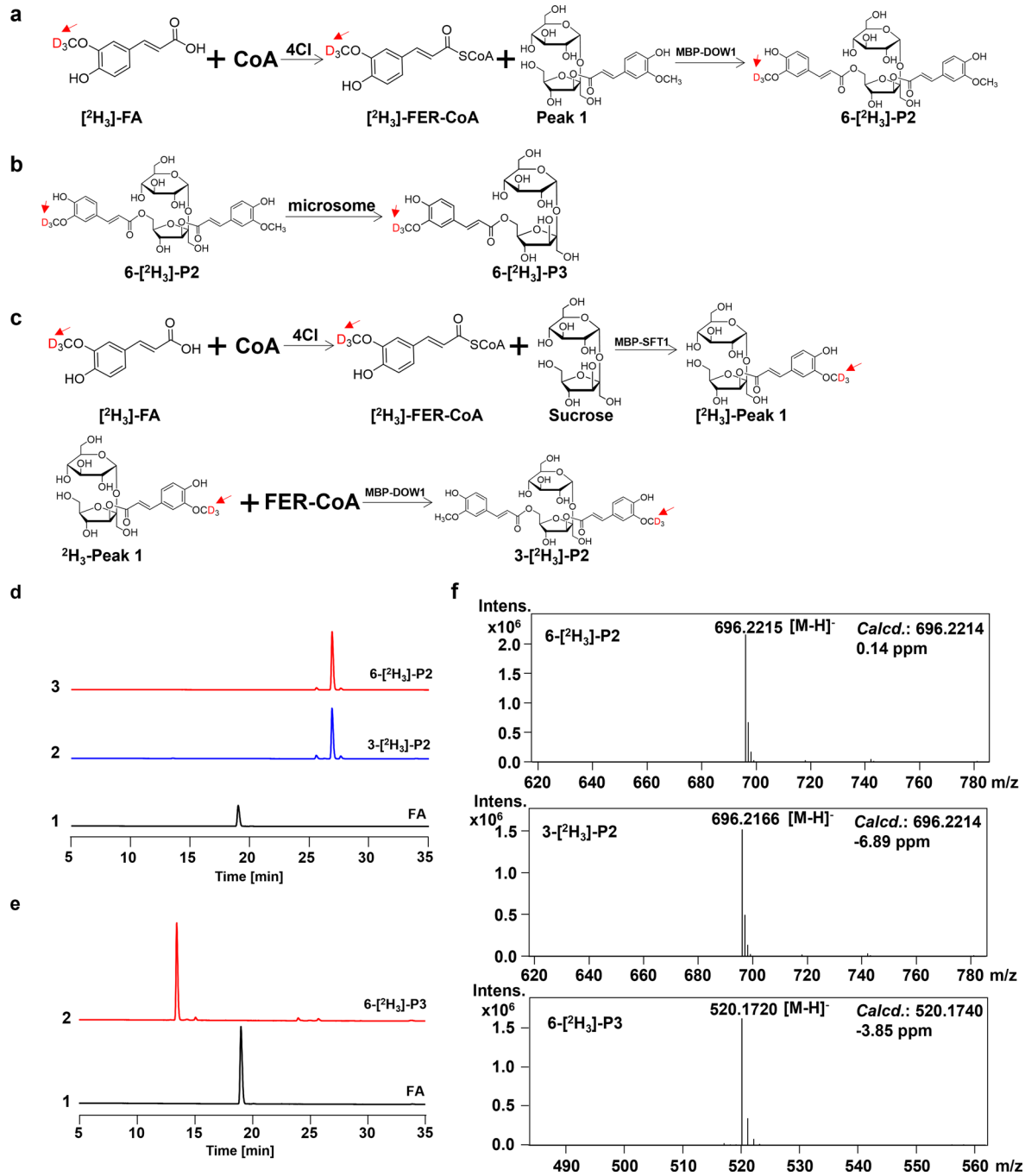

Extended Data Fig. 3 | Preparations of 6-[$^2H_3$]-P2, 6-[$^2H_3$]-P3 and 3-[$^2H_3$]-P2. **a**, Preparation of 6-[$^2H_3$]-P2. **b**, Preparation of 6-[$^2H_3$]-P3. **c**, Preparation of 3-[$^2H_3$]-P2. [$^2H_3$]-FA: [$^2H_3$]-ferulic acid, [$^2H_3$]-Fer-CoA: [$^2H_3$]-feruloyl-CoA. **d**, HPLC analysis of 21.58 uM [$^2H_3$]-FA (*trace 1*), 21.58 uM 6-[$^2H_3$]-P2 (*trace 2*), and 21.58 uM 3-[$^2H_3$]-P2 (*trace 3*). **e**, HPLC analysis of 18.69 uM [$^2H_3$]-FA (*trace 1*) and 18.69 uM 6-[$^2H_3$]-P3 (*trace 2*). These three labeled compounds were used for the subsequent labeling experiment. **f**, HPLC-HR-MS spectra analysis of 6-[$^2H_3$]-P2, 3-[$^2H_3$]-P2, and 6-[$^2H_3$]-P3. For 6-[$^2H_3$]-P2, 3-[$^2H_3$]-P2 and 6-[$^2H_3$]-P3, *m/z* 696.2215, 696.2288, 520.1832 corresponding to [M-H]$^-$ respectively. For unlabelled Peak 2 and Peak 3, the observed *m/z* of [M-H]$^-$ are 693.2003 and 517.1568, respectively.

https://doi.org/10.1038/s41477-024-01781-1

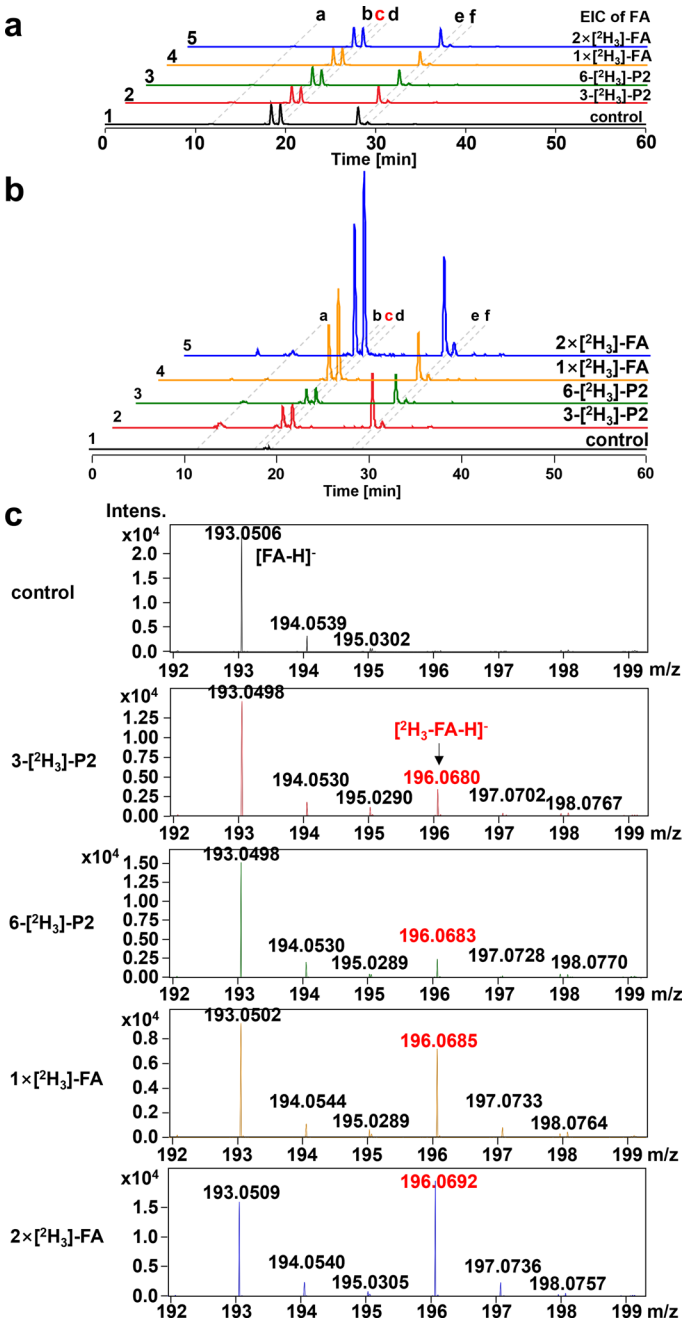

Extended Data Fig. 4 | HPLC-HR-MS analysis of cell wall esterified FA from 3-[$^2H_3$]-P2, 6-[$^2H_3$]-P2 and [$^2H_3$]-FA treatment groups and control. a, EIC of cell wall esterified FA (193.0495, $C_{10}H_9O_4$, [M-H]$^-$) from control (1), and 13.9 μM 3-[$^2H_3$]-P2 (2), 13.9 μM 6-[$^2H_3$]-P2 (3), 13.9 μM [$^2H_3$]-FA (4) and 27.8 μM [$^2H_3$]-FA (5) treatment groups. **b**, EIC of cell-wall esterified [$^2H_3$]-FA (196.0684, $C_{10}H_6D_3O_4$, [M-H]$^-$) from traces unlabeled controls (*trace 1*), and seedlings fed with 13.9 μM 3-[$^2H_3$]-P2 (2), 13.9 μM 6-[$^2H_3$]-P2 (3), 13.9 μM [$^2H_3$]-FA (4), or 27.8 μM [$^2H_3$]-FA (5). The ion chromatogram marked red is selected to show the observed mass spectra of FA from the control and the treatment groups (**c**). **c**, Mass spectra of FA (*Calcd.* of $C_{10}H_9O_4$ is 193.0495, [M-H]$^-$) and [$^2H_3$]-FA (*Calcd.* of $C_{10}H_6D_3O_4$ is 196.0684, [M-H]$^-$) from the control and 13.9 μM 3-[$^2H_3$]-P2, 13.9 μM 6-[$^2H_3$]-P2, 13.9 μM [$^2H_3$]-FA and 27.8 μM [$^2H_3$]-FA treatment groups.

https://doi.org/10.1038/s41477-024-01781-1

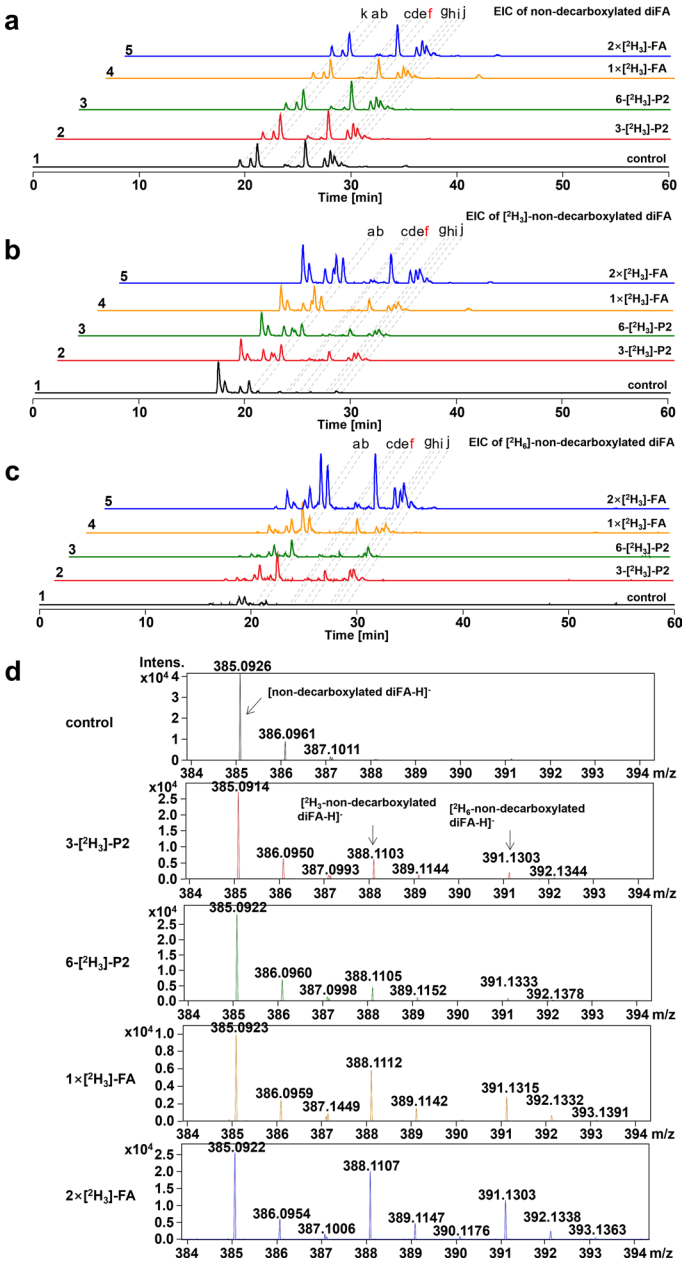

Extended Data Fig. 5 | HPLC-HR-MS analysis of cell wall esterified non-decarboxylated diFA from 3-[$^2H_3$]-P2, 6-[$^2H_3$]-P2, [$^2H_3$]-FA treatment groups and control. a, EIC of non-decarboxylated di-FA (385.0918, $C_{20}H_{17}O_8$, $[M\text{-}H]^-$). a-k refers to the EIC of non-decarboxylated di-FA. **b**, EIC of single FA-labeled non-decarboxylated diFA ([$^2H_3$]-non-decarboxylated diFA) (388.1106, $C_{20}H_{14}D_3O_8$, $[M\text{-}H]^-$). a–j: EIC from treatment groups compared to control. **c**, EIC of double FA-labeled non-decarboxylated diFA ([$^2H_6$]-non-decarboxylated diFA) (391.1295, $C_{20}H_{11}D_6O_8$, $[M\text{-}H]^-$). a–j: EIC from treatment groups compared to control. 1: control; 2 to 5: 13.9 μM 3-[$^2H_3$]-P2, 13.9 μM 6-[$^2H_3$]-P2, 13.9 μM [$^2H_3$]-FA and 27.8 μM [$^2H_3$]-FA treatment groups. Ion chromatogram marked red is selected to show the observed mass spectra of non-decarboxylated di-FA, [$^2H_3$]-non-decarboxylated diFA, and [$^2H_6$]-non-decarboxylated diFA from control and the treatment groups (**d**). **d**, Mass spectra of non-decarboxylated diFA (*Calcd.* of $C_{20}H_{17}O_8$ is 385.0918, $[M\text{-}H]^-$), [$^2H_3$]-non-decarboxylated diFA (*Calcd.* of $C_{20}H_{14}D_3O_8$ is 388.1106, $[M\text{-}H]^-$), [$^2H_6$]-non-decarboxylated diFA (*Calcd.* of $C_{20}H_{11}D_6O_8$ is 391.1295, $[M\text{-}H]^-$) from control and 13.9 μM 3-[$^2H_3$]-P2, 13.9 μM 6-[$^2H_3$]-P2, 13.9 μM [$^2H_3$]-FA, 27.8 μM [$^2H_3$]-FA treatment groups.

https://doi.org/10.1038/s41477-024-01781-1

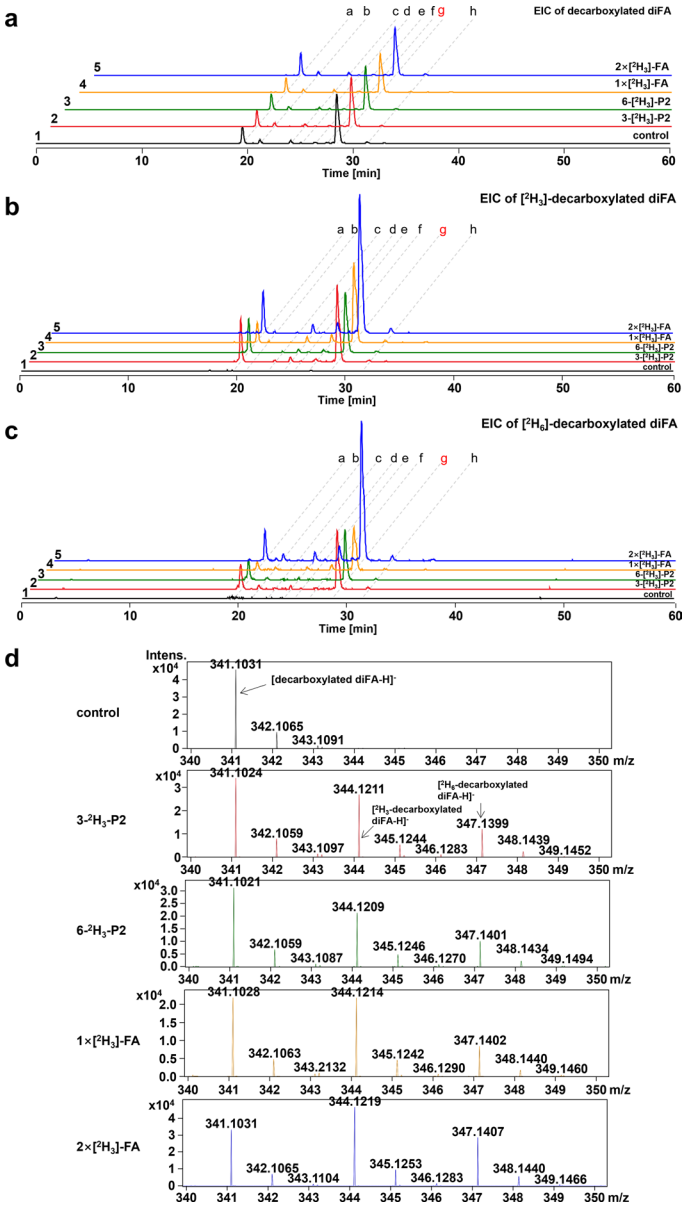

Extended Data Fig. 6 | HPLC-HR-MS analysis of cell wall esterified decarboxylated diFA from 3-[$^2H_3$]-P2, 6-[$^2H_3$]-P2, [$^2H_3$]-FA treatment groups and control. a, EIC of decarboxylated diFA (341.1020, $C_{19}H_{17}O_6$, $[M\text{-}H]^-$). a-h: refer to EIC of decarboxylated diFA. **b**, EIC of single FA-labeled decarboxylated diFA ([$^2H_3$]-decarboxylated diFA) (344.1208, $C_{19}H_{14}D_3O_6$, $[M\text{-}H]^-$). **c**, EIC of double FA-labeled decarboxylated diFA ([$^2H_6$]-decarboxylated diFA) (347.1396, $C_{19}H_{11}D_6O_6$, $[M\text{-}H]^-$). 1: control; 2 to 5: 13.9 μM 3-[$^2H_3$]-P2, 13.9 μM 6-[$^2H_3$]-P2, 13.9 μM [$^2H_3$]-FA and 27.8 μM [$^2H_3$]-FA treatment groups. a-h: EIC from treatment groups compared to control. Ion chromatogram marked red is selected to show the observed mass spectra of [$^2H_3$]-decarboxylated diFA and [$^2H_6$]-decarboxylated diFA from the control and the treatment groups (**d**). **d**, Mass spectra of decarboxylated diFA (*Calcd*. of $C_{19}H_{17}O_6$ is 341.1020, $[M\text{-}H]^-$), [$^2H_3$]-decarboxylated diFA (*Calcd*. of $C_{19}H_{14}D_3O_6$ is 344.1028, $[M\text{-}H]^-$), [$^2H_6$]-decarboxylated diFA (*Calcd*. of $C_{19}H_{11}D_6O_6$ is 347.1396, $[M\text{-}H]^-$) from control and 13.9 μM 3-[$^2H_3$]-P2, 13.9 μM 6-[$^2H_3$]-P2, 13.9 μM [$^2H_3$]-FA and 27.8 μM [$^2H_3$]-FA treatment groups.

https://doi.org/10.1038/s41477-024-01781-1

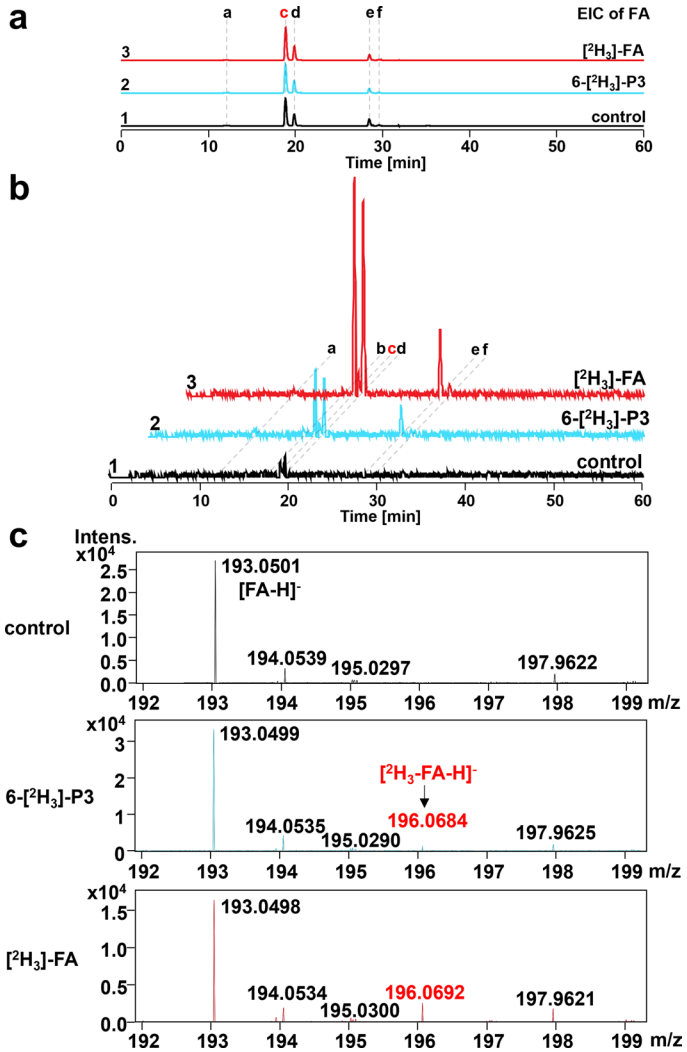

Extended Data Fig. 7 | HPLC-HR-MS analysis of cell wall esterified FA from 6-[$^2H_3$]-P3, and [$^2H_3$]-FA treatment groups and control. a, EIC of cell wall esterified FA from control (1), 6.95 μM 6-[$^2H_3$]-P3 (2), and 6.95 μM [$^2H_3$]-FA (3) treatment groups. c: *trans*-FA; d: *cis*-FA. The ion chromatogram marked red is selected to show the observed mass spectra of FA from the control and the treatment groups (**c**). **b**, The EIC of cell-wall esterified [$^2H_3$]-FA from control seedlings (1) and 6.95 μM 6-[$^2H_3$]-P3 (2), 6.95 μM [$^2H_3$]-FA (3) treatments. The ion chromatogram marked red shows the observed mass spectra of [$^2H_3$]-FA fed seedlings (**c**). c: *trans*-FA; d: *cis*-FA. **c**, Mass spectra of FA (*Calcd*. of $C_{10}H_9O_4$ is 193.0495, $[M\text{-}H]^-$), and [$^2H_3$]-FA (*Calcd*. of $C_{10}H_6D_3O_4$ is 196.0684, $[M\text{-}H]^-$) from control and 6.95 μM 6-[$^2H_3$]-P3, 6.95 μM [$^2H_3$]-FA treatment groups.

https://doi.org/10.1038/s41477-024-01781-1

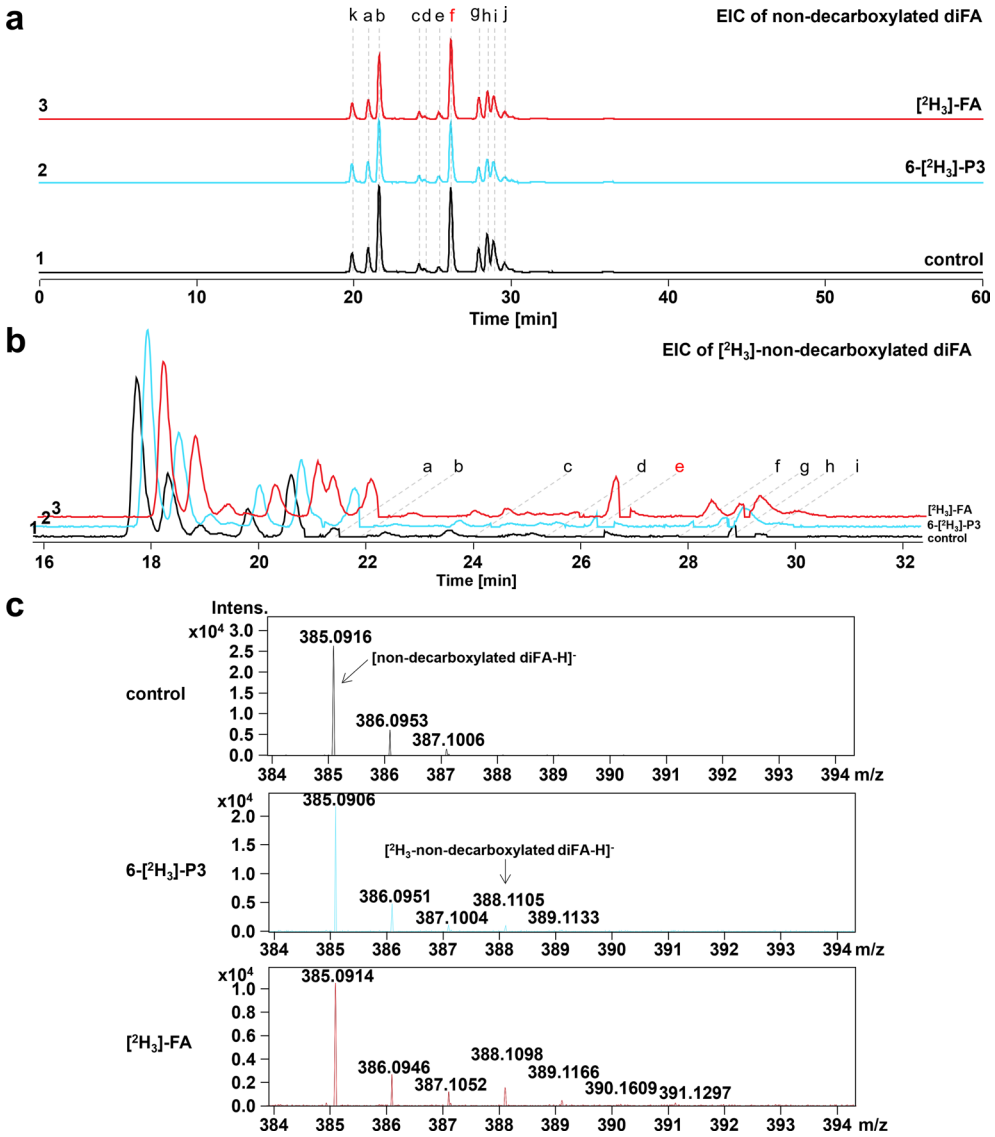

Extended Data Fig. 8 | HPLC-HR-MS analysis of cell wall esterified non-decarboxylated diFA from 6-[$^2H_3$]-P3, [$^2H_3$]-FA treatment groups and control. **a**, EIC of non-decarboxylated diFA (385.0918, $C_{20}H_{17}O_8$, $[M\text{-}H]^-$). a-k refers to non-decarboxylated diFA. **b**, EIC of [$^2H_3$]-non-decarboxylated diFA (388.1106, $C_{20}H_{14}D_3O_8$, $[M\text{-}H]^-$). a-i: EIC from treatments groups compared to control. 1: control; 2: 6.95 μM 6-[$^2H_3$]-P3 treatment group; 3: 6.95 μM [$^2H_3$]-FA treatment group. Ion chromatogram marked red is selected to show the observed mass spectra of non-decarboxylated diFA and [$^2H_3$]-non-decarboxylated diFA from the control and the treatment groups (**c**). **c**, Mass spectra of non-decarboxylated diFA (*Calcd.* of $C_{20}H_{17}O_8$ is 385.0918, $[M\text{-}H]^-$), and [$^2H_3$]-non-decarboxylated diFA (*Calcd.* of $C_{20}H_{14}D_3O_8$ is 388.1106, $[M\text{-}H]^-$) from control and 6.95 μM 6-[$^2H_3$]-P3, 6.95 μM [$^2H_3$]-FA treatment groups.

https://doi.org/10.1038/s41477-024-01781-1

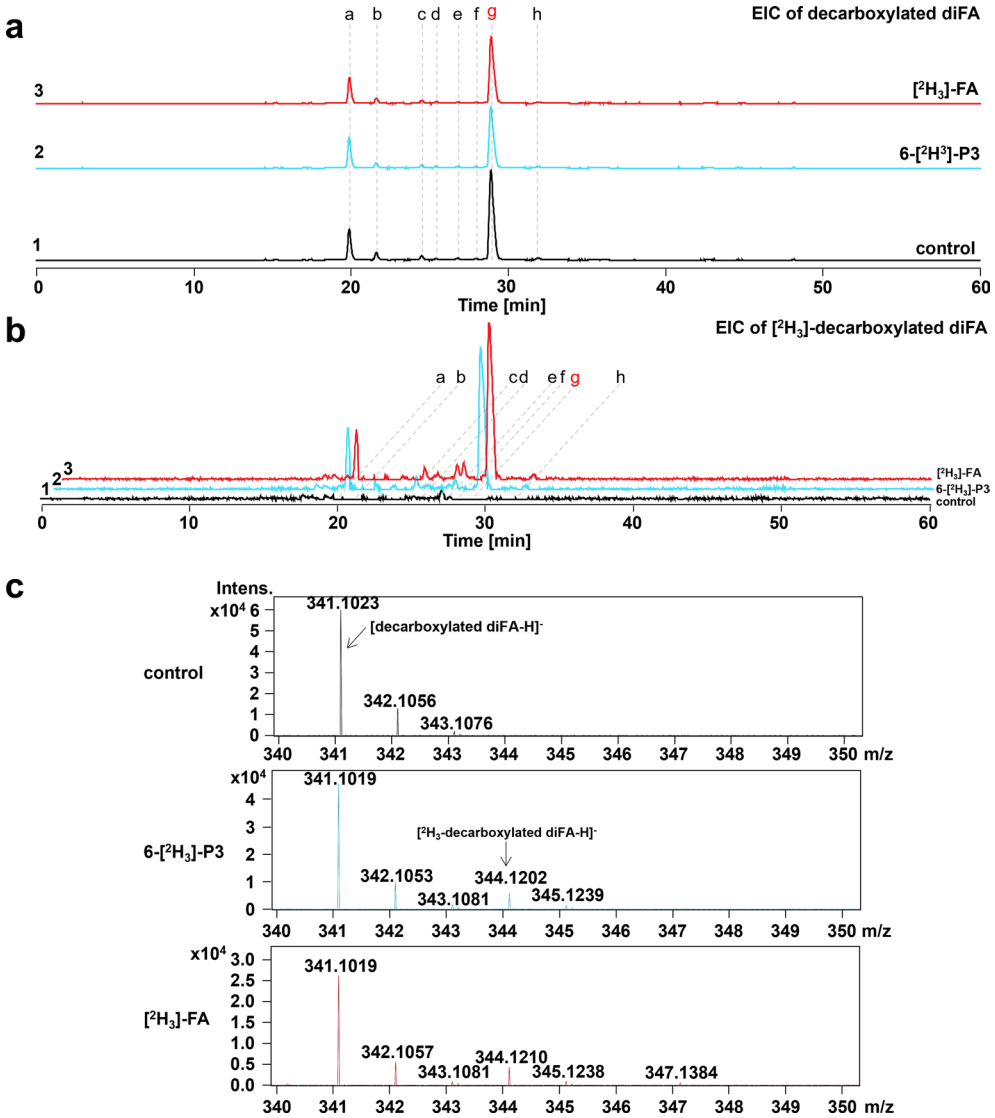

Extended Data Fig. 9 | HPLC-HR-MS analysis of cell wall esterified decarboxylated diFA from 6-[$^2H_3$]-P3, [$^2H_3$]-FA treatment groups and control. a, EIC of decarboxylated diFA (341.1020, $C_{19}H_{17}O_6$, $[M\text{-}H]^-$). a-h refers to decarboxylated diFA. **b**, EIC of [$^2H_3$]-decarboxylated diFA (344.1208, $C_{19}H_{14}D_3O_6$, $[M\text{-}H]^-$). a-h: EIC from treatment groups compared to control. 1: control; 2: 6.95 μM 6-[$^2H_3$]-P3 treatment group; 3: 6.95 μM [$^2H_3$]-FA treatment group. Ion chromatogram marked red is selected to show the observed mass spectra of decarboxylated diFA and [$^2H_3$]-decarboxylated diFA from the control and the treatment groups (**c**). **c**, Mass spectra of decarboxylated diFA (*Calcd.* of $C_{19}H_{17}O_6$ is 341.1020, $[M\text{-}H]^-$), and [$^2H_3$]-decarboxylated diFA (*Calcd.* of $C_{19}H_{14}D_3O_6$ is 344.1028, $[M\text{-}H]^-$) from control and 6.95 μM 6-[$^2H_3$]-P3, 6.95 μM [$^2H_3$]-FA treatment groups.

https://doi.org/10.1038/s41477-024-01781-1

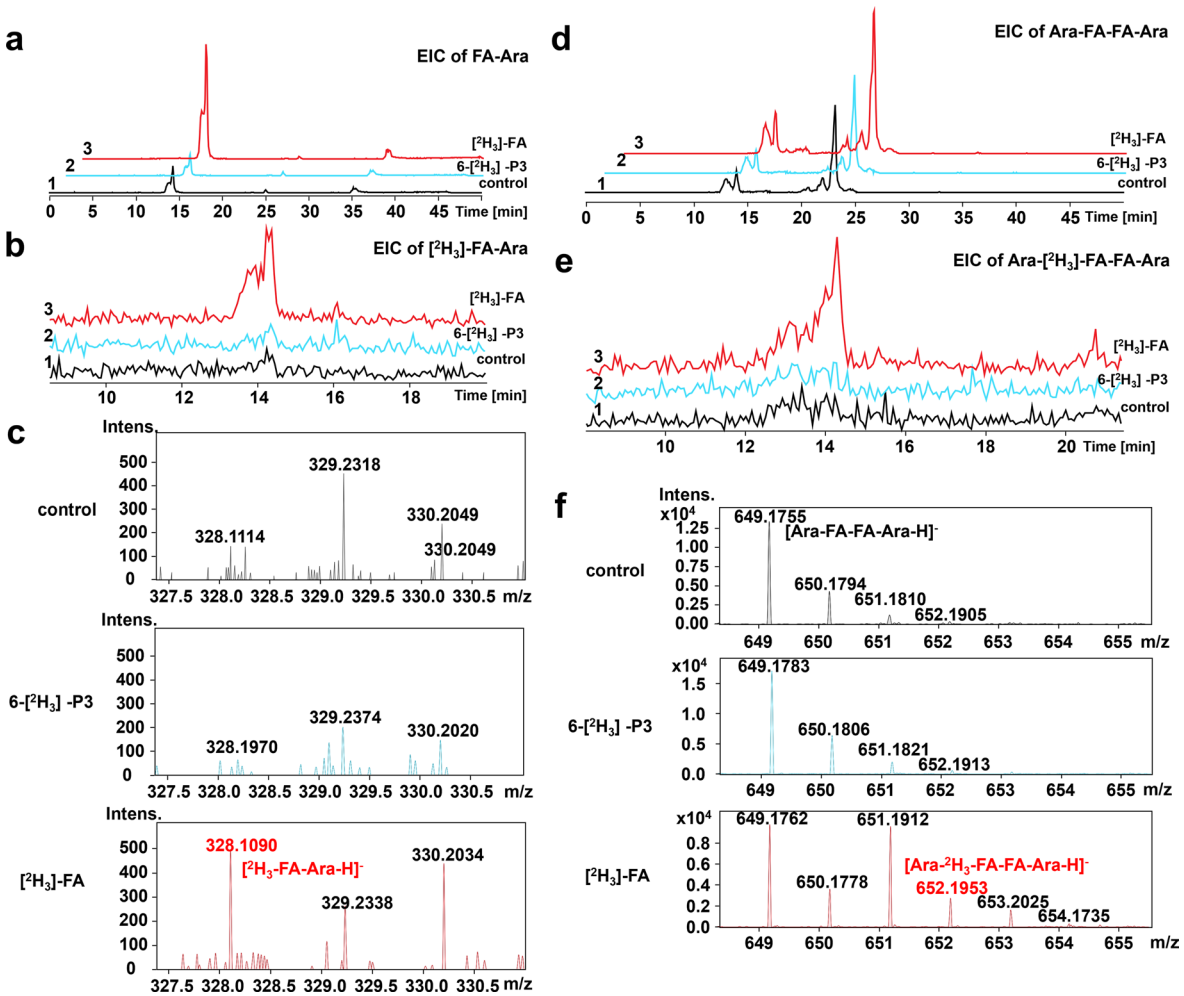

Extended Data Fig. 10 | HPLC-MS analysis of root cell wall hydroxycinnamate (HCA) conjugates from the control and 6-[$^2H_3$]-P3, [$^2H_3$]-FA treatment groups by the 50 mM TFA mild acidolysis method. a, EIC of cell wall FA-Ara (325.0918, $C_{15}H_{18}O_8$, [M-H]$^-$) from control (1) and 6.95 μM 6-[$^2H_3$]-P3 (2), 6.95 μM [$^2H_3$]-FA (3) treatment groups. **b**, EIC of [$^2H_3$]-FA-Ara (328.1106, $C_{15}H_{15}D_3O_8$, [M-H]$^-$) from control (1) and 6.95 μM 6-[$^2H_3$]-P3 (2), 6.95 μM [$^2H_3$]-FA (3) treatment groups. **c**, Mass spectra of [$^2H_3$]-FA-Ara (328.1106, $C_{15}H_{15}D_3O_8$, [M-H]$^-$) from control and 6.95 μM 6-[$^2H_3$]-P3, 6.95 μM [$^2H_3$]-FA treatment groups. **d**, EIC of cell wall Ara-FA-FA-Ara (649.1763, $C_{30}H_{34}O_{16}$, [M-H]$^-$) from the control (1) and 6.95 μM 6-[$^2H_3$]-P3 (2), 6.95 μM [$^2H_3$]-FA (3) treatment groups. **e**, EIC of Ara-[$^2H_3$]-FA-FA-Ara (652.1905, $C_{30}H_{31}D_3O_{16}$, [M-H]$^-$) from the control (1) and 6.95 μM 6-[$^2H_3$]-P3 (2), 6.95 μM [$^2H_3$]-FA (3) treatment groups. **f**, Mass spectra of Ara-[$^2H_3$]-FA-FA-Ara (652.1905, $C_{30}H_{31}D_3O_{16}$, [M-H]$^-$) from the control (1) and 6.95 μM 6-[$^2H_3$]-P3 (2), 6.95 μM [$^2H_3$]-FA (3) treatment groups.

nature portfolio

Corresponding author(s): Bao-Cai Tan

Last updated by author(s): Jul 2, 2024

Reporting Summary

Nature Portfolio wishes to improve the reproducibility of the work that we publish. This form provides structure for consistency and transparency in reporting. For further information on Nature Portfolio policies, see our Editorial Policies and the Editorial Policy Checklist.

Statistics

For all statistical analyses, confirm that the following items are present in the figure legend, table legend, main text, or Methods section.

n/a	Confirmed	
☐	☒	The exact sample size (*n*) for each experimental group/condition, given as a discrete number and unit of measurement
☐	☒	A statement on whether measurements were taken from distinct samples or whether the same sample was measured repeatedly
☐	☒	The statistical test(s) used AND whether they are one- or two-sided *Only common tests should be described solely by name; describe more complex techniques in the Methods section.*
☒	☐	A description of all covariates tested
☒	☐	A description of any assumptions or corrections, such as tests of normality and adjustment for multiple comparisons
☐	☒	A full description of the statistical parameters including central tendency (e.g. means) or other basic estimates (e.g. regression coefficient) AND variation (e.g. standard deviation) or associated estimates of uncertainty (e.g. confidence intervals)
☐	☒	For null hypothesis testing, the test statistic (e.g. *F*, *t*, *r*) with confidence intervals, effect sizes, degrees of freedom and *P* value noted *Give P values as exact values whenever suitable.*
☒	☐	For Bayesian analysis, information on the choice of priors and Markov chain Monte Carlo settings
☒	☐	For hierarchical and complex designs, identification of the appropriate level for tests and full reporting of outcomes
☒	☐	Estimates of effect sizes (e.g. Cohen's *d*, Pearson's *r*), indicating how they were calculated

Our web collection on statistics for biologists contains articles on many of the points above.

Software and code

Policy information about availability of computer code

Data collection	Maize embryo cell wall was observed using transmission electron microscope (Thermo Scientific, FEI Tecnai G2 F20). The fluorescence signal was detected using a confocal microscope (Zeiss, LSM900). HPLC separation was carried out using a Shimadzu LC-20AT HPLC equipped with a diode array detector SPD-M20A. Compounds were prepared using a Shimadzu LC-6AD semi-preparative liquid chromatography. NMR spectra were recorded on a Bruker Avance III 600 MHz spectrometer. HPLC-HR–MS/MS was performed on a rapid separation liquid chromatography system (Dionex, UltiMate3000, UHPLC) coupled with an ESI-Q-TOF mass spectrometer (Bruker Daltonics, Impact HD).
Data analysis	Statistical analysis: GraphPad Prism (version 9.0.2) NMR data were processed by using the MestReNova software (14.0.0) HPLC-HR-MS and HPLC-HR-MS/MS data were analyzed using the DataAnalysis software (Bruker Daltonics)

For manuscripts utilizing custom algorithms or software that are central to the research but not yet described in published literature, software must be made available to editors and reviewers. We strongly encourage code deposition in a community repository (e.g. GitHub). See the Nature Portfolio guidelines for submitting code & software for further information.

Data

Policy information about availability of data

All manuscripts must include a data availability statement. This statement should provide the following information, where applicable:

- Accession codes, unique identifiers, or web links for publicly available datasets
- A description of any restrictions on data availability
- For clinical datasets or third party data, please ensure that the statement adheres to our policy

All data are available in this article and its Extended Data Figures and Supplementary Figures and Tables.

Human research participants

Policy information about studies involving human research participants and Sex and Gender in Research.

Reporting on sex and gender	N/A
Population characteristics	N/A
Recruitment	N/A
Ethics oversight	N/A

Note that full information on the approval of the study protocol must also be provided in the manuscript.

Field-specific reporting

Please select the one below that is the best fit for your research. If you are not sure, read the appropriate sections before making your selection.

☒ Life sciences ☐ Behavioural & social sciences ☐ Ecological, evolutionary & environmental sciences

For a reference copy of the document with all sections, see nature.com/documents/nr-reporting-summary-flat.pdf

Life sciences study design

All studies must disclose on these points even when the disclosure is negative.

Sample size	Sample size was determined based on previous publications on similar experiments. Previous publication considered to determine sample size include: Cell wall ester-linked p-coumaric acid and ferulic acid analysis (doi: 10.1111/nph.14970)
Data exclusions	No data were excluded.
Replication	All experiments were repeated at least two or three times, and the number of biological replicates is indicated in the figure legends.
Randomization	Plants were randomly assigned to the treatment and control groups with no formal randomization techniques.
Blinding	Researchers were not blinded to the allocation during experiments. The research materials are plants, so the blind design is not applicable to all experiments. Experiments were performed using routine practice and repeated by different authors. All samples were labeled with an identifier that revealed their identities. Blinding was not relevant as the samples were processed randomly through experimental procedures.

Reporting for specific materials, systems and methods

We require information from authors about some types of materials, experimental systems and methods used in many studies. Here, indicate whether each material, system or method listed is relevant to your study. If you are not sure if a list item applies to your research, read the appropriate section before selecting a response.

Materials & experimental systems

n/a	Involved in the study
☐	☒ Antibodies
☒	☐ Eukaryotic cell lines
☒	☐ Palaeontology and archaeology
☒	☐ Animals and other organisms
☒	☐ Clinical data
☒	☐ Dual use research of concern

Methods

n/a	Involved in the study
☒	☐ ChIP-seq
☒	☐ Flow cytometry
☒	☐ MRI-based neuroimaging

Antibodies

Antibodies used

anti-DOW1
anti-histone H3 (sc-374669, Santa Cruz)
anti-BiP (AS09 481, Agrisera)
anti-PIP1 (AS09 505, Agrisera)

Validation

The polyclonal anti-DOW1 antibody was raised and screened by authors in this article. The polyclonal anti-DOW1 antibody was validated in Western blot analysis on maize total proteins from 7-day-old seedlings, 15 days after pollination wild-type maize embryos, and 15 days after pollination dow1-1 and dow1-2 mutant embryos.

Anti-histone H3 (https://www.scbt.com/p/p-histone-h3-antibody-c-2) Anti-histone H3 antibody was validated by the Vendor (Santa Cruz) by Western Blotting. It is recommended for the detection of Histone H3 in mice, rats, humans, Drosophila, Xenopus, C. elegans, and other animals.

Anti-BiP (https://www.agrisera.com/en/artiklar/bip2-luminal-binding-protein-2.html) The anti-Bip antibody was validated by the Vendor (Agrisera) via immunoblotting analysis on total proteins from maize.

Anti-PIP1 (https://www.agrisera.com/en/artiklar/pip1s-aquaporin-.html) The anti-PIP1 antibody was validated by the Vendor (Agrisera) via immunoblotting analysis on crude membrane fraction/lane from Oryza sativa.